Tang T., Zhang Y., Dong B., & Huang L. (2024). Computation of acoustic scattered fields and derived radiation force and torque for axisymmetric objects at arbitrary orientations. *Journal of the Acoustical Society of America*.
DOI: 10.1121/10.0032405

Computation of acoustic scattered fields and derived radiation force and torque for axisymmetric objects at arbitrary orientations

Tianquan Tang,[1, a)] Yumin Zhang,[1] Bin Dong,[2, b)] and Lixi Huang[3]

[1)]*School of Mechatronic Engineering and Automation, Foshan University, 33 Guangyun Road, Nanhai District, Foshan, China*[c)]

[2)]*High Speed Aerodynamics Institute, China Aerodynamics Research and Development Center, Mianyang, China*

[3)]*Department of Mechanical Engineering, The University of Hong Kong, Pokfulam, Hong Kong SAR, China*

This study presents a theoretical framework for calculating acoustic scattering fields, as well as radiation force and torque resulting from the interaction between an incident wave and an axisymmetric object positioned at arbitrary orientations. Grounded in the partial-wave expansion method, it formulates scattering products using beam-shape and scalar scattering coefficients. The incorporation of geometric features into the scalar scattering coefficients is achieved through conformal transformation approach. Notably, its applicability is restricted to scenarios where the object is positioned at its standard orientation, a limitation circumvented by employing rotational transformations to extend the model to non-standard orientations. A rotational transformation tunes the original frame [observation coordinate system, OCS] into a reference frame [computation coordinate system, CCS], compensating for any deviated orientation and facilitating solution of scattering products. While the non-intuitive nature of rotational transformations disrupts the inheritability of the partial-wave expressions for the scattering products, an alternative approach is provided based on rotation addition theorem. This method directly incorporates object orientations into the beam-shape and scalar scattering coefficients, bypassing rotational transformations and preserving the partial-wave format. Comparative analysis with full 3D numerical simulations shows theoretical methods are computationally more efficient while ensuring substantial consistency.

[a)]corresponding author: tianquan@connect.hku.hk

[b)]nudt18214@163.com

[c)]Also at Lab for Aerodynamics and Acoustics, HKU Zhejiang Institute of Research and Innovation, 1623 Dayuan Road, Lin An District, Hangzhou, China

I. INTRODUCTION

The precise manipulation of micro-objects is a crucial capability for studies involving cells and microorganisms, as well as for applications in biotechnology in general[1]. Acoustic methods have emerged as potential tools for effectively manipulating objects[2,3]. The general analytical expressions for acoustic radiation force and torque exert on objects because of the momentum and angular momentum transfers, respectively, that arise from acoustic scattering effects of the wave-particle interaction were given subsequently by Westervelt and Mardanik in 1950s[4–6]. An alternative expression to evaluate the acoustic radiation torque was provided by Fan[7], and the relation with Maidaniks formulation was carefully discussed by Zhang and Marston[8]. Different from the Gorkov potential theory, which is commonly employed to manipulate Rayleigh objects dominated by monopole and dipole scattering[9,10], through decomposing the external and scattering fields as the partial-wave expansion series[11] and inserting them into the formulations provided by Westervelt and Mardanik, the higher-order scattering contributions from complex objects can be accounted for, making this method suitable for both Rayleigh and Mie scattering regimes.

For spherical objects, explicit expressions for the acoustic radiation force and torque are derived based on the expansion coefficients. Within the spherical coordinate system, the boundary conditions of spherical particles and the orthogonality of spherical wavefunctions are employed to decouple each mode and obtain a system of linear equations for the unknown scattering field, thereby determining the radiation force and torque[12–16]. While an analytical model exists for the radiation force and torque in spherical geometries, few theories can effectively quantify the impact of non-spherical geometrical features on scattering properties, including acoustic radiation force and torque. Actually, affected by the acoustic radiation pressure, the shape of the levitated spherical droplet is flattened to be an oblate spheroidal object[17,18]. Further experiments demonstrated that the non-spherical shape parameter can be regarded as an additional degree of freedom for particle manipulation that remains largely unexplored[19,20]. For a vortex beam propagating along the symmetric axis of the objects, an general analytical framework for acoustic radiation torque on an axisymmetric absorbing object suggested that the axial radiation torque exerted by the non-paraxial acoustic vortex beam[21] on such an object is directly proportional to the power absorbed by the object[22], and the relationship between the radiation torque and viscous dissipation was also established[23]. In on-axis cases, the direction of the radiation torque and consequently the spin of an axisymmetric object are determined by the helicity of the vortex beam. However, in illumina-

tion of an off-axis-located object by vortex waves, a radiation torque could spin an axisymmetric object around its center of mass in a direction opposite to the wave vortex's handedness, and this reversal effect depends on the offset distance of the off-axis object away from the core of the beam[24]. When dealing with non-spherical objects, the radial distance to any point on the object surface depends on angular coordinates, and the spherical wavefunctions may not be necessarily orthogonal. This complexity makes closed-form exact solutions of the scattering field challenging within the spherical coordinate system. Within the partial-wave framework, explicit expressions quantifying the acoustic radiation force and torque on prolate spheroids can be derived by introducing a surface shape function to accurately formulate the boundary conditions[25,26]. Additional insights and connections were further explored in Ref.[27] Another accessible method to calculate the radiation force and torque on a prolate spheroid is to directly analyse the problem within the spheroidal coordinate system so that the radial distance to any point on the object surface is a constant[28]. For general axisymmetric geometries, a natural approach is to analyse the problem within their asymptotical (quasi-spherical) coordinate system, allowing the boundary condition to be expressed solely by the radial coordinates. In this context, the use of conformal mapping becomes valuable for transforming the physical surface of geometries into a spherical surface under a quasi-spherical coordinate system[29,30]. This approach ensures that the locus of all points corresponding to the mapped radial coordinate being constant aligns with the scatterer surface, facilitating the enforcement of boundary conditions. Consequently, the separation of variables can be employed to solve the mapped Helmholtz wave equation, subject to the boundary conditions[31–33]. Moreover, this strategy ensures consistency and logical coherence with the approach employed to address spherical geometries, thereby demonstrating robust inheritability.

Although the conformal transformation approach can be utilized to calculate the scattering products of axisymmetric objects, it is only valid when the symmetric axis of the objects coincides with one of the coordinate axes in Cartesian coordinate system. Once the orientation of the axisymmetric object changes, breaking the axisymmetric condition, the approach becomes invalid. Considering that the orientations of axisymmetric objects constantly change under the influence of radiation torque, it is necessary to extend the framework to make the approach applicable in different orientations. Naturally, the rotation of the particle can be treated as the opposite rotation of the external field, achieved by employing a rotational transformation to adjust the external field. Mathematically, this case is equivalent to the external field being at rest while the particle rotates[34–36]. However, the rotational transformation and its reverse are cumbersome and

non-intuitive. More importantly, due to the existence of both direct and reverse rotational transformations, the scattering acoustic field cannot be directly expressed as a partial-wave expansion series. This implies that the analytical formulations for acoustic radiation force and torque will also include rotational transformation processes, making it challenging to represent them directly as a series of expansion coefficients. This disrupts the inheritability of the partial-wave framework, hindering its subsequent extension, such as its potential application to multi-object systems for evaluating the interaction radiation force and torque. In this study, we aim to introduce a compact alternative that directly incorporates the effect of rotations on the expansion coefficients, i.e., the beam-shape coefficients and the scattering coefficients, utilizing the addition theorem[37], which ensures the retainment of partial-wave inheritability.

Prior to the study, it is essential to establish the coordinate systems and define the rotational principles for subsequent use. To ensure consistency with the work[34], we define an observation coordinate system (OCS) where the origin coincides with the center of mass of the manipulated particle, denoted as (x', y', z') system, which is acceptable as an absolute coordinate system to further discuss the dynamic problem since it is established under the well-known Cartesian coordinate system. By contrast, a computation coordinate system (CCS), denoted as (x, y, z) system, is introduced to better characterize the axisymmetric particle. The origin of these two systems is spatially coincident, while the z-axis of the computation system is defined by the symmetric axis of the particle. Note that both sets of axes, $Ox'y'z'$ and $Oxyz$, are right-handed system and these two systems are depicted in Fig. 1(a). We further define the *standard orientation* of an axisymmetric object as the alignment of its symmetric axis with the z-axis (or z'-axis) within the corresponding coordinate system. It has been observed that the particle naturally aligns with the standard orientation within the CCS. This inherent alignment serves as the fundamental basis for implementing the conformal transformation approach within the CCS, as discussed in Sec. II. Suppose that the OCS [or $Ox'y'z'$] is rotated into the CCS [or $Oxyz$] through three successive finite rotations, quantified by three Eulerian angles α, β, and γ, which are defined as [the *finite rotational principles*]: (i) rotate (particle) anti-clockwise by about the z'-axis. This takes the y'-axis into a new line called the line of nodes; (ii) rotate (particle) anti-clockwise by about the line of nodes. This takes the z'-axis into the z-axis; (iii) rotate (particle) anti-clockwise by about the z-axis. This takes the line of nodes into the y-axis (thus the x'-axis is finally projected into the x-axis). The prescription 'anti-clockwise' denotes a positive angle under the right-handed rule. In Secs. III and IV, we introduce the theoretical frameworks for predicting the acoustic scattering fields resulting from

the interaction of an incident wave with axisymmetric objects at arbitrary orientations, utilizing the rotational transformation and the rotation addition theorem, respectively. Subsequently, the radiation force and torque exerted on the objects are formulated based on the obtained scattering fields. Results and discussions are presented in Sec. V, followed by comprehensive validations against full three-dimensional numerical simulations. A summary is made in Sec. VI.

II. SCATTERING PROBLEM OF AXISYMMETRIC GEOMETRIES

A. Conformal transformation approach

A time-harmonic wave of angular frequency ω is described by a velocity potential function $\hat{\phi}\mathrm{e}^{-\mathrm{i}\omega \mathrm{t}}$, where r denotes position vector with respect to the system origin and t is time. In the source-free regions of the physical space, the total velocity potential amplitude $\hat{\phi}\left(\vec{r}\right)$ [denoted as $\hat{\phi}$] satisfies the Helmholtz wave equation

$$\left(\nabla^2 + k^2\right)\hat{\phi} = 0, \tag{1}$$

where ∇^2 is the Laplacian operator. The time-dependent term $\mathrm{e}^{-\mathrm{i}\omega \mathrm{t}}$ is omitted for the sake of simplicity. The total potential amplitude includes the external potential amplitude $\hat{\phi}_{\mathrm{ex}}\left(\vec{r}\right)$ [denoted as $\hat{\phi}_{\mathrm{ex}}$] and the scattering potential amplitude reflected by the scatterer $\hat{\phi}_{\mathrm{sc}}\left(\vec{r}\right)$ [denoted as $\hat{\phi}_{\mathrm{sc}}$],

$$\hat{\phi} = \hat{\phi}_{\mathrm{ex}} + \hat{\phi}_{\mathrm{sc}}. \tag{2}$$

We consider a time-harmonic acoustic wave with arbitrary wavefront interacting with an axisymmetric object. The linearity of the problem allows us to represent the external field with wavenumber k as a partial-wave series as[11]

$$\hat{\phi}_{\mathrm{ex}} = \sum_{n,m} a_{nm} J_n^m, \tag{3}$$

where the hat symbol $\hat{}$ represents the complex amplitude of the corresponding variable. Abbreviation $\sum_{n,m} \equiv \sum_{n=0}^{\infty}\sum_{m=-n}^{+n}$. Abbreviation variable J_n^m defines as a function $J_n^m\left(k\vec{r}\right) \equiv j_n\left(kr\right)Y_n^m\left(\theta,\phi\right)$ with $\vec{r} = \left(r,\theta,\phi\right)$ in terms of the spherical coordinate system. $j_n\left(kr\right)$ is the spherical Bessel function of order n at a position r, and $Y_n^m\left(\theta,\phi\right)$ is the spherical harmonic function of n-th order and

m-th degree at the angular position (θ, ϕ).

For any external wave satisfies the homogeneous Helmholtz equation, the method of quadratures stands out as the direct and intuitive approach for isolating the beam-shape coefficients, denoted generally as a_{nm}. This is achieved by leveraging the orthogonality properties inherent in spherical harmonics[34,38]:

$$a_{nm} = \frac{1}{j_n(k\mathrm{R})} \int_0^{2\pi} \int_0^{\pi} \hat{\phi}_{\mathrm{anyl}}\left(\vec{\mathrm{R}}\right) Y_n^m(\theta,\phi)^* \sin\theta \mathrm{d}\theta \mathrm{d}\phi, \tag{4}$$

where $\vec{\mathrm{R}} = (\mathrm{R}, \theta, \phi)$ specifies a spherical space with a radius of R that encompasses the scatterer but not the sound sources. $\hat{\phi}_{\mathrm{anyl}}\left(\vec{\mathrm{R}}\right)$ is the analytical expression of the (external) potential amplitude at the surface $\vec{\mathrm{R}}$. The asterisk symbol * means taking conjugation of the corresponding variable.

Correspondingly, the scattering potential amplitude derives from any axisymmetric object can be expressed in terms of a partial-wave series as:

$$\hat{\phi}_{\mathrm{sc}} = \sum_{n,m} a_{nm} s_{nm} H_n^m, \tag{5}$$

where s_{nm} are the scalar scattering coefficients, depending on the geometric features. Function $H_n^m \equiv H_n^m(k\vec{r}) \equiv h_n^{(1)}(kr) Y_n^m(\theta,\phi)$. $h_n^{(1)}(kr)$ is the first kind of spherical Hankel function of order n at a position r. For the sound-soft and sound-hard boundary conditions, the scalar scattering coefficients are obtained, respectively, by solving the following equations[31]

$$\begin{aligned} &\sum_{n=0}^{\infty} a_{nm'} \Gamma_n^{n',m'} + \sum_{n=0}^{\infty} s_{nm'} a_{nm'} \Lambda_n^{n',m'} = 0, \\ &(n' = 0, 1, \cdots, \infty; m' = -\infty, \cdots, 0, \cdots, \infty) \end{aligned} \tag{6}$$

and

$$\begin{aligned} &\sum_{n=0}^{\infty} a_{nm'} \Gamma_{n,u}^{n',m'} + \sum_{n=0}^{\infty} s_{nm'} a_{nm'} \Lambda_{n,u}^{n',m'} = 0, \\ &(n' = 0, 1, \cdots, \infty; m' = -\infty, \cdots, 0, \cdots, \infty) \end{aligned} \tag{7}$$

Here, the structural functions, $\Gamma_n^{n',m'}$ and $\Lambda_n^{n',m'}$, and their partial derivatives $\Gamma_{n,u}^{n',m'}$ and $\Lambda_{n,u}^{n',m'}$, are

$$\begin{cases} \Gamma_n^{n',m'} = \int_0^{2\pi}\int_0^{\pi} j_n\left(kr(u,w)\right) Q_n^m P_n^{m'}\left(\cos\theta(u,w)\right) P_{n'}^{m'}\left(\cos w\right)\sin w \mathrm{d}w\mathrm{d}v\Big|_{u=u_0} \\ \Lambda_n^{n',m'} = \int_0^{2\pi}\int_0^{\pi} h_n\left(kr(u,w)\right) Q_n^m P_n^{m'}\left(\cos\theta(u,w)\right) P_{n'}^{m'}\left(\cos w\right)\sin w \mathrm{d}w\mathrm{d}v\Big|_{u=u_0} \\ \Gamma_{n,u}^{n',m'} = \frac{\partial \Gamma_n^{n',m'}}{\partial u}\Big|_{u=u_0} \\ \Lambda_{n,u}^{n',m'} = \frac{\partial \Lambda_n^{n',m'}}{\partial u}\Big|_{u=u_0} \end{cases}, \tag{8}$$

where $P_{n'}^{m'}(\cdot)$ represents the associated Legendre function of n'-th order and m'-th degree for the variable therein, and $Q_n^m = \sqrt{\frac{(2n+1)}{4\pi}\frac{(n-m)!}{(n+m)!}}$.

In evaluation of the structure functions in Eq. (8), we need to provide the conformal mapping relationship between the physical space (r,θ,ϕ) and the mapping coordinates (u,w,v)[31]. Specifically, for any axisymmetric object, a general three-dimensional geometry can be equivalently described by a two-dimensional cross-sectional slice plane (u and w) and an azimuthal coordinate variable (v). Since the profile of any cross-sectional slice is identical, the geometric features depend solely on the cross-sectional slice. Here, conformal transformation method is employed to map the slice into a quasi-spherical coordinate system, in where the locus of all points of the slice boundary is equal to a constant ($u = u_0$), and the spherical coordinates r, θ, and ϕ are connected with the mapping coordinates u, w, and v by

$$\begin{cases} r(u,w) = \sqrt{f(u,w)^2 + g(u,w)^2} \\ \theta(u,w) = \cos^{-1}\left(g(u,w)/r(u,w)\right) \\ \phi = v \end{cases}, \tag{9}$$

with the mapping functions $g(u,w)$ and $f(u,w)$ as

$$\begin{cases} g(u,w) = c_{-1}\mathrm{e}^u\cos(w) + \sum_{n=0}^{\infty} c_n \mathrm{e}^{-nu}\cos(nw) \\ f(u,w) = c_{-1}\mathrm{e}^u\sin(w) - \sum_{n=0}^{\infty} c_n \mathrm{e}^{-nu}\sin(nw) \end{cases}, \tag{10}$$

where the mapping coefficients c_n are used to map the physical coordinate system to the mapping (quasi-spherical) coordinate systems [referred to Appendix A of our previous work[31] for the determination of mapping coefficients]. Finally, by inserting the structural functions ($\Gamma_n^{n',m'}$, $\Lambda_n^{n',m'}$, $\Gamma_{n,u}^{n',m'}$, $\Lambda_{n,u}^{n',m'}$), and the beam-shape coefficients (a_{nm}) into matrices (6) or (7), the unknown scalar

scattering expansion coefficients (s_{nm}) of the non-spherical particle are determined.

It should be emphasized that the potential amplitude [$\hat{\phi}_{\rm ex}$, $\hat{\phi}_{\rm sc}$, and $\hat{\phi}$] are directly dependent on the mapping coordinates (u,w,v) through position vector $\vec{r}=(r(u,w),\theta(u,w),\phi)$ in Eq. (9). While consider the constraint for each mapping coordinates (u,w,v), there should be only a set of one-to-one correspondance spherical coordinates (r,θ,ϕ). In this way, the potential amplitude can be also regarded as the direct functions of position vector $\vec{r}=(r,\theta,\phi)$ with respect to the spherical coordinate system.

B. Acoustic radiation force and torque

After calculating both the external and scattered acoustic fields through the partial-wave expansion method, the radiation force and torque can be derived as a surface integration of the object as[31]

$$\begin{cases} \vec{F}_{\rm rad}=\frac{\rho_0\omega^2}{c_0^2}\int_{\rm R}\left[\langle\phi_{\rm ex}\phi_{\rm sc}\rangle\,\vec{e}_r+\langle\phi_{\rm sc}\phi_{\rm sc}\rangle\,\vec{e}_r+\left\langle\frac{{\rm i}c_0}{\omega}\phi_{\rm sc}\nabla\phi_{\rm sc}\right\rangle\right]{\rm dA_R} \\ \vec{T}_{\rm rad}=-\rho_0\int_{\rm R}\left\langle{\rm i}\frac{\partial(\phi_{\rm ex}+\phi_{\rm sc})}{\partial r}\vec{K}(\phi_{\rm ex}+\phi_{\rm sc})\right\rangle{\rm dA_R} \end{cases}, \tag{11}$$

where ρ_0 and c_0 are the density and speed of sound of the host fluid, respectively. Angle bracket $\langle\cdot\rangle$ denotes the time average of the variable therein. Note that the spherical surface R surrounding the scattering particle should be sufficiently far to involve the scatterer, and the direction of the a unit vector $\vec{e}_r$ is along the outer normal of the surface. $\vec{K}=-{\rm i}\,(\vec{r}\times\nabla)$ representing the angular momentum operator[39]. We can eliminate the time-averaged effects of the potential field using relationship $\langle\phi_{\rm ex}\phi_{\rm sc}\rangle=\frac{1}{2}{\rm Re}\left(\hat{\phi}_{\rm ex}\hat{\phi}_{\rm sc}^{*}\right)$, and thus the radiation force and torque can be obtained by inserting the potential amplitude [Eqs. (3) and (5)] into Eq. (11). A detailed derivative is given in Appendix A. Consequently, the Cartesian components of the radiation force and torque exerted on any axisymmetric object can be expressed as[14,36]

$$\begin{cases} F_{{\rm rad},x}={\rm Re}\left[\frac{{\rm i}\rho_0}{4}\sum_{n,m}a_{nm}\,(1+s_{nm})\left(\mathscr{A}_{n+1}^{m+1}b_{n+1,m+1}^{*}-\mathscr{B}_{n-1}^{m+1}b_{n-1,m+1}^{*}+\mathscr{C}_{n+1}^{m-1}b_{n+1,m-1}^{*}-\mathscr{D}_{n-1}^{m-1}b_{n-1,m-1}^{*}\right)\right] \\ F_{{\rm rad},y}={\rm Re}\left[\frac{\rho_0}{4}\sum_{n,m}a_{nm}\,(1+s_{nm})\left(\mathscr{A}_{n+1}^{m+1}b_{n+1,m+1}^{*}-\mathscr{B}_{n-1}^{m+1}b_{n-1,m+1}^{*}-\mathscr{C}_{n+1}^{m-1}b_{n+1,m-1}^{*}+\mathscr{D}_{n-1}^{m-1}b_{n-1,m-1}^{*}\right)\right] \\ F_{{\rm rad},z}={\rm Re}\left[\frac{{\rm i}\rho_0}{2}\sum_{n,m}a_{nm}\,(1+s_{nm})\left(\mathscr{E}_{n+1}^{m}b_{n+1,m}^{*}-\mathscr{F}_{n-1}^{m}b_{n-1,m}^{*}\right)\right] \end{cases}, \tag{12}$$

and

$$\begin{cases} T_{\mathrm{rad},x} = \mathrm{Re}\left[\frac{\rho_0}{4k}\sum_{n,m} a_{nm}\left(1+s_{nm}\right)\left(\mathscr{G}_n^m b_{n,m+1}^* + \mathscr{G}_n^{-m} b_{n,m-1}^*\right)\right] \\ T_{\mathrm{rad},y} = -\mathrm{Re}\left[\frac{\mathrm{i}\rho_0}{4k}\sum_{n,m} a_{nm}\left(1+s_{nm}\right)\left(\mathscr{G}_n^m b_{n,m+1}^* - \mathscr{G}_n^{-m} b_{n,m-1}^*\right)\right] \\ T_{\mathrm{rad},z} = \mathrm{Re}\left[\frac{\rho_0}{2k}\sum_{n,m} a_{nm}\left(1+s_{nm}\right) m b_{n,m}^*\right] \end{cases}, \tag{13}$$

where $b_{nm} = a_{nm}s_{nm}$ defined as the scattering coefficients, and symbol Re means taking the real part of the expression. The weighting coefficients $\mathscr{A}_n^m = -\mathscr{C}_n^{-m} = -\sqrt{\frac{(n+m-1)(n+m)}{(2n-1)(2n+1)}}$, $\mathscr{B}_n^m = -\mathscr{D}_n^{-m} = \sqrt{\frac{(n-m+2)(n-m+1)}{(2n+1)(2n+3)}}$, $\mathscr{E}_n^m = \mathscr{F}_{n-1}^m = \sqrt{\frac{(n-m)(n+m)}{(2n-1)(2n+1)}}$, and $\mathscr{G}_n^m = \sqrt{(n-m)\left(n+m+1\right)}$.

III. RADIATION FORCE AND TORQUE: USING ROTATIONAL TRANFORMATION

A. Rotational tranformation of external products

Generally, the CCS does not align with the OCS, and the orientational deviation of the CCS [denoted as $Oxyz$] from the OCS [denoted as $Ox'y'z'$] can be precisely quantified by considering finite rotational effects, as shown in Fig. 1(a). The rotational effect is characterized by $\vec{\theta}_{\mathrm{rot}} = (\alpha, \beta, \gamma)$, where α, β, and γ denote the rotational angles around the respective axes. The finite rotational principles are elaborated upon in the *Introduction*. Mathematically, the coordinate variables between the CCS and the OCS can be mutually expressed with the help of the rotational transformation matrices[40] as:

$$\mathbf{R}_1(\alpha) = \begin{bmatrix} \cos(\alpha) & -\sin(\alpha) & 0 \\ \sin(\alpha) & \cos(\alpha) & 0 \\ 0 & 0 & 1 \end{bmatrix}, \mathbf{R}_2(\beta) = \begin{bmatrix} \cos(\beta) & 0 & \sin(\beta) \\ 0 & 1 & 0 \\ -\sin(\beta) & 0 & \cos(\beta) \end{bmatrix}, \mathbf{R}_3(\gamma) = \begin{bmatrix} \cos(\gamma) & -\sin(\gamma) & 0 \\ \sin(\gamma) & \cos(\gamma) & 0 \\ 0 & 0 & 1 \end{bmatrix}. \tag{14}$$

To incorporate geometric features into our calculations, we intend to utilize the conformal transformation approach. However, the conformal transformation approach discussed in Sec. II is only applicable when the particle remains in the standard orientation, i.e., within the CCS. Note that the expression of external field, $\hat{\phi}_{\mathrm{anyl}}$, is typically formulated in the OCS. From the perspective of the CCS, the external field can be conceptualized as undergoing a rotational transformation of $-\vec{\theta}_{\mathrm{rot}}$ around the origin of the CCS. Therefore, an 'opposite' rotational transformation (i.e., by $-\vec{\theta}_{\mathrm{rot}}$) is applied on the external field, which allows us to simulate the effects of the external field

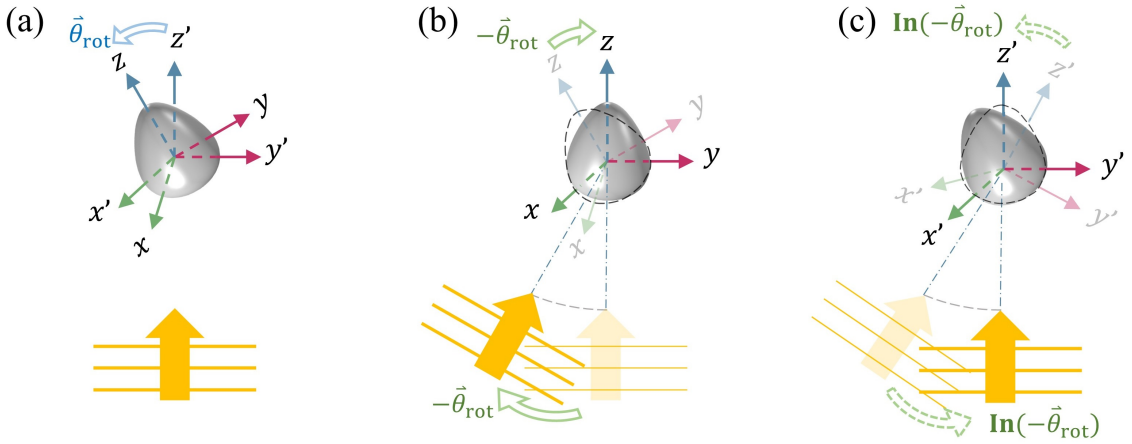

FIG. 1. (a) Geometric description of the position relationship between the OCS [denoted as Cartesian system $Ox'y'z'$] and the CCS [denoted as Cartesian system $Oxyz$]. The CCS is derived from the OCS through three finite rotational effects, quantified by rotation angles $\vec{\theta}_{\text{rot}} = (\alpha, \beta, \gamma)$. (b) A rotational transformation $-\vec{\theta}_{\text{rot}}$ is needed to rotate the acoustic external field within the CCS. (c) A reverse rotational transformation $\mathbf{In}(-\vec{\theta}_{\text{rot}})$ is employed to recover the expressions of the scattering products within the OCS.

within the CCS. As depicted in Fig. 1(b). The rotated external potential amplitude is expressed as

$$\begin{cases} \hat{\phi}_{\text{anyl}}^{\text{CCS,RT}} &= \hat{\phi}_{\text{anyl}}(x', y', z') \\ [x', y', z'] &= [x, y, z] \cdot \mathbf{R}_1(-\alpha)\mathbf{R}_2(-\beta)\mathbf{R}_3(-\gamma) \end{cases}, \tag{15}$$

with the superscripts $^{\text{CCS}}$ and $^{\text{RT}}$ represent the computation coordinate system and the rotational transformation products, respectively. As a result, the corresponding beam-shape coefficients are accessible by Eq. (4) as

$$a_{nm}^{\text{CCS,RT}} = \frac{1}{j_n(k\text{R})} \int_0^{2\pi} \int_0^{\pi} \hat{\phi}_{\text{anyl}}^{\text{CCS,RT}}\left(\vec{\text{R}}\right) Y_n^m(\theta, \phi)^* \sin\theta \text{d}\theta \text{d}\phi. \tag{16}$$

Consequently, we are able to obtain the scalar scattering coefficients for sound-soft boundary condition with respect to the CCS, $s_{nm}^{\text{CCS,RT}}$, through inserting $a_{nm}^{\text{CCS,RT}}$ into matrix (6) and solving it [or solving Eq. (7) for sound-hard boundary condition]. In this way, the scattering potential amplitude on the CCS can be expressed as $\hat{\phi}_{\text{sc}}^{\text{CCS,RT}} = \sum_{n,m} s_{nm}^{\text{CCS,RT}} a_{nm}^{\text{CCS,RT}} H_n^m$. The corresponding radiation force and torque, $\vec{F}_{\text{rad}}^{\text{CCS,RT}} = \left[F_{\text{rad},x}^{\text{CCS,RT}}, F_{\text{rad},y}^{\text{CCS,RT}}, F_{\text{rad},z}^{\text{CCS,RT}}\right]$ and $\vec{T}_{\text{rad}}^{\text{CCS,RT}} = \left[T_{\text{rad},x}^{\text{CCS,RT}}, T_{\text{rad},y}^{\text{CCS,RT}}, T_{\text{rad},z}^{\text{CCS,RT}}\right]$, are given in Eqs. (12) and (13) while replace a_{nm} and s_{nm} with $a_{nm}^{\text{CCS,RT}}$ and $s_{nm}^{\text{CCS,RT}}$, respectively.

B. Reverse rotational transformation of scattering products

Following calculations within the CCS to obtain the acoustic scattered field, radiation force, and torque, we subsequently apply an reverse rotational transformation to acquire the corresponding values in the OCS. From the standpoint of the OCS, the scattering products can be conceptualized as undergoing an reverse rotational transformation [denoted as $\mathbf{In}(-\vec{\theta}_{\mathrm{rot}})$ with symbol **In** indicating reverse] around the origin of the OCS, as depicted in Fig. 1(c). As a result, the scattering potential amplitude becomes

$$\begin{cases} \hat{\phi}_{\mathrm{sc}}^{\mathrm{OCS,RT}} &= \hat{\phi}_{\mathrm{sc}}^{\mathrm{CCS,RT}}(x,y,z) \\ [x,y,z] &= [x',y',z'] \cdot \mathbf{R}_3^{-1}(\gamma)\,\mathbf{R}_2^{-1}(\beta)\,\mathbf{R}_1^{-1}(\alpha) \end{cases}, \tag{17}$$

the radiation force and torque are given as

$$\vec{F}_{\mathrm{rad}}^{\mathrm{OCS,RT}} = \vec{F}_{\mathrm{rad}}^{\mathrm{CCS,RT}} \cdot \mathbf{R}_3^{-1}(\gamma)\,\mathbf{R}_2^{-1}(\beta)\,\mathbf{R}_3^{-1}(\alpha), \tag{18}$$

and

$$\vec{T}_{\mathrm{rad}}^{\mathrm{OCS,RT}} = \vec{T}_{\mathrm{rad}}^{\mathrm{CCS,RT}} \cdot \mathbf{R}_3^{-1}(\gamma)\,\mathbf{R}_2^{-1}(\beta)\,\mathbf{R}_3^{-1}(\alpha), \tag{19}$$

with the superscript $^{\mathrm{OCS}}$ indicates the observation coordinate system. In this way, the scattered potential amplitude, radiation force, and torque acting upon an axisymmetric particle with an arbitrary orientation can be calculated.

IV. RADIATION FORCE AND TORQUE: USING ROTATION METRICS

A. Rotation of beam-shape coefficients

As mentioned previously, the rotation from the OCS to the CCS is described by $\vec{\theta}_{\mathrm{rot}} = (\alpha,\beta,\gamma)$. Similarly, to proceed with the conformal transformation, the axisymmetric particle must be positioned in its standard orientation, i.e., within the CCS. Therefore, it is necessary to rotate the external field by an angle of $-\vec{\theta}_{\mathrm{rot}} = (-\alpha,-\beta,-\gamma)$ to maintain the incident angle of the external field and the orientation of the particle unchanged [referred to Fig. 1(b)]. Differing from the approach based on rotational transformation, a more concise approach involves directly rotating the

spherical harmonics using rotation matrices[37]. Specifically, we have

$$\begin{aligned}\hat{\phi}_{\mathrm{ex}}^{\mathrm{CCS,RM}} &= \sum_{n=0}^{\infty}\sum_{m=-n}^{+n} a_{nm} j_n(kr) \sum_{l=-n}^{+n} D_n^{m,l}(-\vec{\theta}_{\mathrm{rot}}) Y_n^l(\theta,\phi) \\ &= \sum_{n=0}^{\infty}\sum_{l=-n}^{+n} \left[\sum_{m=-n}^{+n} a_{nm} D_n^{m,l}(-\vec{\theta}_{\mathrm{rot}})\right] j_n(kr) Y_n^l(\theta,\phi) \\ &= \sum_{n=0}^{\infty}\sum_{m=-n}^{+n} \left[\sum_{l=-n}^{+n} a_{nl} D_n^{l,m}(-\vec{\theta}_{\mathrm{rot}})\right] j_n(kr) Y_n^m(\theta,\phi) \\ &= \sum_{n,m} a_{nm}^{\mathrm{CCS,RM}} J_n^m, \end{aligned} \tag{20}$$

where the superscript $^{\mathrm{RM}}$ represents the products based on the rotation addition theorem using rotation matrices, and the corresponding beam-shape coefficients becomes

$$a_{nm}^{\mathrm{CCS,RM}} = \sum_{l=-n}^{+n} a_{nl} D_n^{l,m}(-\vec{\theta}_{\mathrm{rot}}). \tag{21}$$

In the above equations, $D_n^{m,l}(\vec{\theta})$ is defined as the elements of rotation matrices. An explicit formula for $D_n^{m,l}(\vec{\theta})$ can be found in Appendix B. Then, we can bring coefficients $a_{nm}^{\mathrm{CCS,RM}}$ into matrices (6) and (7) for the corresponding scalar scattering coefficients ($s_{nm}^{\mathrm{CCS,RM}}$) of the sound-soft and sound-hard boundary conditions, respectively.

B. Reverse rotation of scalar scattering coefficients

To determine the scattering field within the OCS, a reverse rotational effect is needed, as illustrated in Fig. 1(c). Similarly, the reverse rotational effect can be considered conveniently by employing another rotation matrices as:

$$\begin{aligned}\hat{\phi}_{\mathrm{sc}}^{\mathrm{OCS,RM}} &= \sum_{n=0}^{\infty}\sum_{m=-n}^{+n} a_{nm}^{\mathrm{CCS,RM}} s_{nm}^{\mathrm{CCS,RM}} h_n^1(kr') \sum_{l=-n}^{+n} D_n^{m,l}(\mathbf{In}(-\vec{\theta}_{\mathrm{rot}})) Y_n^l(\theta',\phi') \\ &= \sum_{n=0}^{\infty}\sum_{l=-n}^{+n} \left[\sum_{m=-n}^{+n} a_{nm}^{\mathrm{CCS,RM}} s_{nm}^{\mathrm{CCS,RM}} D_n^{m,l}(\mathbf{In}(-\vec{\theta}_{\mathrm{rot}}))\right] h_n^1(kr') Y_n^l(\theta',\phi') \\ &= \sum_{n=0}^{\infty}\sum_{m=-n}^{+n} \left[\sum_{l=-n}^{+n} a_{nl}^{\mathrm{CCS,RM}} s_{nl}^{\mathrm{CCS,RM}} D_n^{l,m}(\mathbf{In}(-\vec{\theta}_{\mathrm{rot}}))\right] h_n^1(kr') Y_n^m(\theta',\phi') \\ &= \sum_{n,m} b_{nm}^{\mathrm{OCS,RM}} H_n^m \end{aligned}$$

$$= \sum_{n,m} a_{nm} s_{nm}^{\mathrm{OCS,RM}} H_n^m, \tag{22}$$

where the rotated scattering coefficients, $b_{nm}^{\mathrm{OCS,RM}}$, and the rotated scalar scattering coefficients, $s_{nm}^{\mathrm{OCS,RM}}$, are

$$\begin{cases} b_{nm}^{\mathrm{OCS,RM}} = \sum\limits_{l=-n}^{+n} a_{nl}^{\mathrm{CCS,RM}} s_{nl}^{\mathrm{CCS,RM}} D_n^{l,m}(\mathbf{In}(-\vec{\theta}_{\mathrm{rot}})) \\ s_{nm}^{\mathrm{OCS,RM}} = \frac{1}{a_{nm}} \sum\limits_{l=-n}^{+n} a_{nl}^{\mathrm{CCS,RM}} s_{nl}^{\mathrm{CCS,RM}} D_n^{l,m}(\mathbf{In}(-\vec{\theta}_{\mathrm{rot}})) \end{cases}. \tag{23}$$

In the above equations, we use the notation $\mathbf{In}(-\vec{\theta}_{\mathrm{rot}}) = (\gamma, \beta, \alpha)$ where convenient, representing the effects of reverse rotations. It is essential to note that, to maintain consistency with the format of Eq. (5), we have extracted the beam-shape coefficients, a_{nm}, from the scattering coefficients $b_{nm}^{\mathrm{OCS,RM}}$, resulting in scalar scattering coefficients, $s_{nm}^{\mathrm{OCS,RM}}$. However, it is crucial to highlight that the denominator of the scalar scattering coefficients is a_{nm}. This implies that when a_{nm} equals zero, $s_{nm}^{\mathrm{OCS,RM}}$ tends towards infinity, rendering the computation infeasible. Considering this aspect, in subsequent calculations, whether for the computation of the scattered acoustic field or the calculation of radiation force and torque, we directly utilize the scattering coefficients $b_{nm}^{\mathrm{OCS,RM}}$ to avoid potential numerical errors. In this manner, referring to Eqs. (12) and (13), the radiation force and torque can be expressed directly in terms of $a_{nm}^{\mathrm{OCS,RM}}$ and $b_{nm}^{\mathrm{OCS,RM}}$ as follows:

$$\begin{cases} F_{\mathrm{rad},x'}^{\mathrm{OCS,RM}} = \mathrm{Re}\left[\frac{\mathrm{i}\rho_0}{4} \sum_{n,m} \left(a_{nm}^{\mathrm{OCS,RM}} + b_{nm}^{\mathrm{OCS,RM}}\right) \left(\mathscr{A}_{n+1}^{m+1} b_{n+1,m+1}^{\mathrm{OCS,RM}} - \mathscr{B}_{n-1}^{m+1} b_{n-1,m+1}^{\mathrm{OCS,RM}} + \mathscr{C}_{n+1}^{m-1} b_{n+1,m-1}^{\mathrm{OCS,RM}} - \mathscr{D}_{n-1}^{m-1} b_{n-1,m-1}^{\mathrm{OCS,RM}}\right)^*\right] \\ F_{\mathrm{rad},y'}^{\mathrm{OCS,RM}} = \mathrm{Re}\left[\frac{\rho_0}{4} \sum_{n,m} \left(a_{nm}^{\mathrm{OCS,RM}} + b_{nm}^{\mathrm{OCS,RM}}\right) \left(\mathscr{A}_{n+1}^{m+1} b_{n+1,m+1}^{\mathrm{OCS,RM}} - \mathscr{B}_{n-1}^{m+1} b_{n-1,m+1}^{\mathrm{OCS,RM}} - \mathscr{C}_{n+1}^{m-1} b_{n+1,m-1}^{\mathrm{OCS,RM}} + \mathscr{D}_{n-1}^{m-1} b_{n-1,m-1}^{\mathrm{OCS,RM}}\right)^*\right] \\ F_{\mathrm{rad},z'}^{\mathrm{OCS,RM}} = \mathrm{Re}\left[\frac{\mathrm{i}\rho_0}{2} \sum_{n,m} \left(a_{nm}^{\mathrm{OCS,RM}} + b_{nm}^{\mathrm{OCS,RM}}\right) \left(\mathscr{E}_{n+1}^{m} b_{n+1,m}^{\mathrm{OCS,RM}} - \mathscr{F}_{n-1}^{m} b_{n-1,m}^{\mathrm{OCS,RM}}\right)^*\right] \end{cases}, \tag{24}$$

and

$$\begin{cases} T_{\mathrm{rad},x'}^{\mathrm{OCS,RM}} = \mathrm{Re}\left[\frac{\rho_0}{4k} \sum_{n,m} \left(a_{nm}^{\mathrm{OCS,RM}} + b_{nm}^{\mathrm{OCS,RM}}\right) \left(\mathscr{G}_n^m b_{n,m+1}^{\mathrm{OCS,RM}} + \mathscr{G}_n^{-m} b_{n,m-1}^{\mathrm{OCS,RM}}\right)^*\right] \\ T_{\mathrm{rad},y'}^{\mathrm{OCS,RM}} = -\mathrm{Re}\left[\frac{\mathrm{i}\rho_0}{4k} \sum_{n,m} \left(a_{nm}^{\mathrm{OCS,RM}} + b_{nm}^{\mathrm{OCS,RM}}\right) \left(\mathscr{G}_n^m b_{n,m+1}^{\mathrm{OCS,RM}} - \mathscr{G}_n^{-m} b_{n,m-1}^{\mathrm{OCS,RM}}\right)^*\right] \\ T_{\mathrm{rad},z'}^{\mathrm{OCS,RM}} = \mathrm{Re}\left[\frac{\rho_0}{2k} \sum_{n,m} \left(a_{nm}^{\mathrm{OCS,RM}} + b_{nm}^{\mathrm{OCS,RM}}\right) \left(m b_{n,m}^{\mathrm{OCS,RM}}\right)^*\right] \end{cases}. \tag{25}$$

In contrast to the method relying on rotational transformations, which directly manipulates the solved acoustic scattering fields, radiation force, and torque [referred to Eqs. (17), (18), and (19)], the scattering products [given in Eqs. (22), (24), and (25)] based on rotation addition theorem can be used to obtain the beam-shape and scalar scattering coefficients relative to the object orientations. This approach preserves inheritability within the partial-wave framework and maintains a

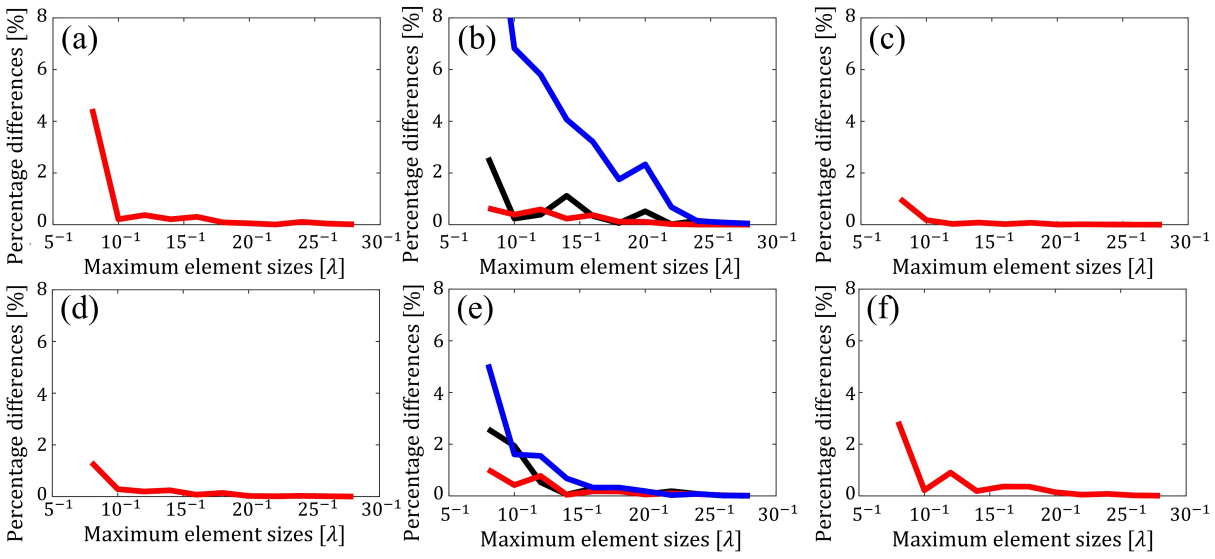

FIG. 2. The percentage difference of acoustic radiation force and torque as a function of maximum element size around the object used in numerical simulations. The red, black, and blue lines denote the distributions of radiation force on the z'-axis, radiation force on the x'-axis, and radiation torque on the y'-axis, respectively. Sub-figures (a), (b), and (c) represent the radiation force/torque on the cone with orientations of 0, $\pi/4$, and $\pi/2$, respectively, while sub-figures (d), (e), and (f) illustrate the radiation force/torque on the disc with the same arrangement. Due to the symmetric properties, the radiation force on the x'-axis and radiation torque on the y'-axis vanish at orientations of 0 and $\pi/2$

more intuitive and compact expressions.

V. RESULTS AND DISCUSSION

A series of comprehensive three-dimensional simulations of wave-particle interactions have been performed to validate the acoustic scattering potential field, radiation force and radiation torque. The simulations are implemented in commercial software COMSOL MULTIPHYSICS. Given that the pressure and the particle velocity can be represented by the potential field as $-\rho_0 \frac{\partial \phi}{\partial t} = p$ and $\nabla \phi = \vec{u}$, the pressure p and particle velocity $\vec{u}$ obtained through numerical simulations allow for the direct calculation of radiation force and torque using Eq. (11) [a detailed derivation is provided in Appendix D of our previous work[31]].

The sound-hard boundary conditions for the different axisymmetric particles (all averaged radius of $a = 50$ μm) with different orientations in water have been simulated. A plane wave with a unit pressure amplitude [or $p_0 = 1$ Pa] is set in COMSOL as a *background pressure field* with the frequency of 12 MHz [or the size parameter $ka \approx 2.5$], proporgating along the $+z'$-axis. The

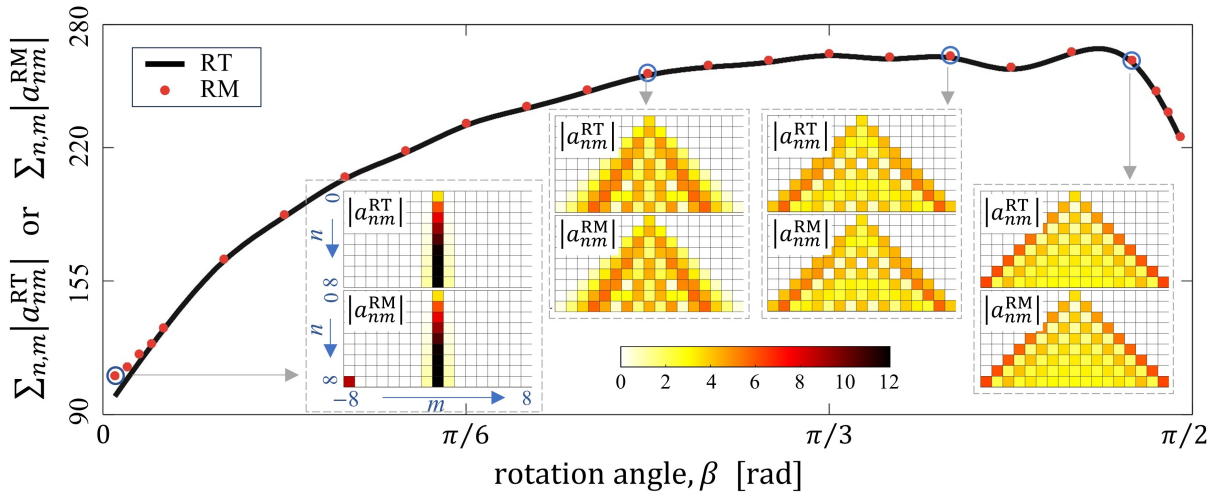

FIG. 3. The summation of absolute values of rotated beam-shape coefficients based on the rotational transformation (RT, $|a_{nm}^{\mathrm{RT}}|$ in Eq. (16)) and the rotation matrices (RM, $|a_{nm}^{\mathrm{RM}}|$ in Eq. (21)) at different rotation angles, β [$\alpha=\gamma=0$]. The inserted contours illustrate the data distribution of $|a_{nm}^{\mathrm{RT}}|$ and $|a_{nm}^{\mathrm{RM}}|$ at $\beta=1^\circ$, 45°, 70° and 85°.

maximum element size is set to $\lambda/6$ in the entire computational domain, while a much denser mesh distribution is necessary on the integration surface surrounding the particles for accurately evaluating of the radiation force and torque. To mitigate the numerical errors, a mesh convergence analysis has been conducted by gradually increasing the mesh density on the integration surface. The percentage difference of acoustic radiation force/torque as a function of maximum element size around the cone/disc with different orientations are listed in Fig. 2. Considering that all values do not vary significantly after $\lambda/25$, we have ultimately set the maximum element size to $\lambda/25$ since further increasing the mesh density does not significantly impact the numerical results. In theoretical calculations, we need to truncate the infinite summation $\sum_{n,m}\equiv\sum_{n=0}^{\infty}\sum_{m=-n}^{+n}$ to $\sum_{n,m}\equiv\sum_{n=0}^{N}\sum_{m=-n}^{+n}$ using a truncation number $N=8$ so that we could perform the predictions of Eqs. (5), (6), (7), (12), (13), (20), (22), (24) and (25) properly[31,35,38]. It is noteworthy that the computational time for each numerical simulation (10 minutes) is considerably higher than the time required in our method (1 second for radiation forces/torques and 1 min for scattering fields using parallel computing) on a standard general personal computer (CPU: Intel i9-13900K 3.0 GHz with 24-core, Maximum memory usage: 128 GB).

A. Comparison of rotated beam-shape coefficients

Figure 3 compares the absolute values of the rotated beam-shape coefficients using both rotational transformation [in Eq. (16)] and rotation matrices [in Eq. (21)] for different rotation angles β [$\alpha = \gamma = 0$], corresponding to the rotation of the $Ox'y'z'$ system about the y'-axis to the $Oxyz$ system. An excellent agreement of the rotated beam-shape coefficients based on the rotation matrices (RM) is observed compared to that based on the rotational transformation (RT). When the object is located at the standard orientation, the rotated beam-shape coefficients, $|a_{nm}^{\mathrm{RT}}|$ and $|a_{nm}^{\mathrm{RM}}|$, are initially confined to the central domain [with $m = 0$], while $|a_{nm}^{\mathrm{RT}}|$ and $|a_{nm}^{\mathrm{RM}}|$ vanish for $m \neq 0$. With the increase of rotation angle β, $|a_{nm}^{\mathrm{RT}}|$ and $|a_{nm}^{\mathrm{RM}}|$ start to spread to the non-central domain [with $m \neq 0$]. Physically, the object deviating from its standard orientation in the OCS is mathematically equivalent to the plane wave undergoing an opposite rotation process within the CCS [referred to Fig. 1]. In order to better approximate the rotated plane wave, additional non-central data is required.

It is noteworthy that the beam-shape coefficients of a plane wave propagating with arbitrary orientation can be analytically expressed as[11]

$$a_{nm}^{\mathrm{anly}} = \mathrm{i}^n 4\pi Y_n^m(\theta_{\mathrm{inc}}, \phi_{\mathrm{inc}})^*, \tag{26}$$

where the polar and azimuthal angles, θ_{inc} and ϕ_{inc}, quantify the propagating orientation. Examining Eq. (26), it is evident that when $\theta_{\mathrm{inc}} = 0$, $Y_n^m(0, \phi_{\mathrm{inc}}) \sim \delta_{m,0}$ [with δ_{nm} the Kronecker Delta] and thus a_{nm}^{anly} is non-zero only when $m = 0$; conversely, when $\theta_{\mathrm{inc}} \neq 0$, non-zero a_{nm}^{anly} will spread to $m \neq 0$, confirming the characteristics of the rotated beam-shape coefficients.

We can also observe a slight deviation in Fig. 3 as β approaches zero. This discrepancy arises during the computation in Eq. (21), where the first step involves evaluating the rotation matrices $D_n^{m,l}(-\vec{\theta}_{\mathrm{rot}})$. However, the determination of the reduced rotation matrices $d_n^{m,l}(-\beta)$, using Eqs. (B9) and (B10), incorporates the evaluation of the term $\left(\tan\frac{\beta}{2}\right)^{2k+l-m}$. It is well-established that as β tends to be zero, the term $\tan\frac{\beta}{2}$ also tends to zero. Consequently, if $2k+l-m \ll 0$, $\left(\tan\frac{\beta}{2}\right)^{2k+l-m}$ tend toward infinity, significant numerical errors may occur. Therefore, when applying rotation matrices to address cases with small rotational angles, it is advisable to maintain a small truncation number N to ensure higher accuracy. It is important to note that the same numerical errors exist when computing the scattering coefficients in Eq. (23).

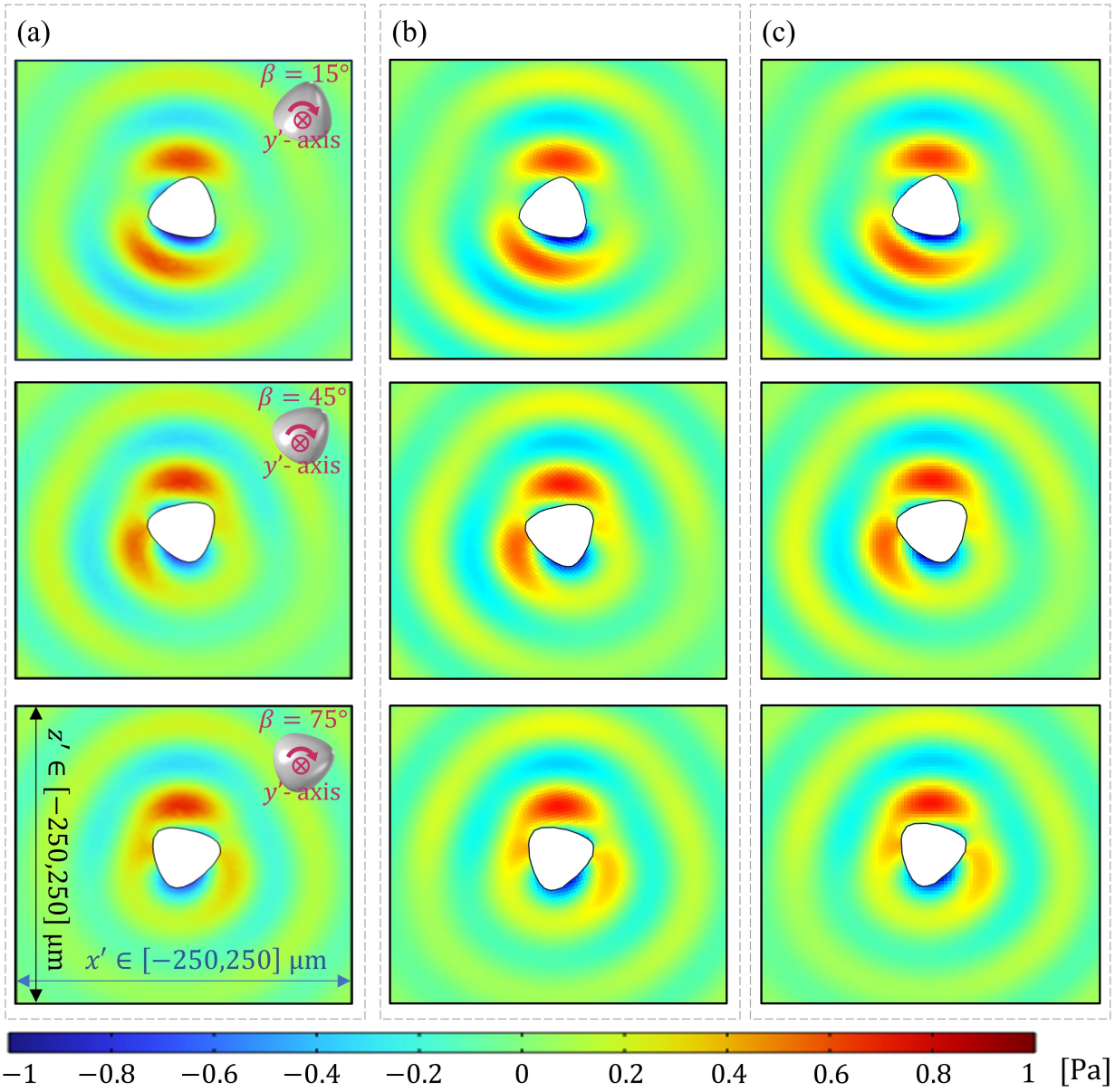

FIG. 4. The pressure amplitude of the acoustic scattering fields generated by a plane wave propagating along the z'-axis with a unit pressure amplitude, interacting with a sound-hard cone-like object undergoing rotations about the y'-axis by $\beta = 15°$, $45°$, and $75°$. The pressure amplitudes are obtained through (a) numerical simulations, and theoretical model incorporating (b) the rotational transformations and (c) the rotation matrices.

B. Comparison of scattering fields

The pressure amplitude of the acoustic scattering fields resulting from a plane interacting with a cone-like and a disc-like object at various orientations are depicted in Figs. 4 and 5, respectively. Note that the potential amplitude of the scattered waves based on rotational transformation

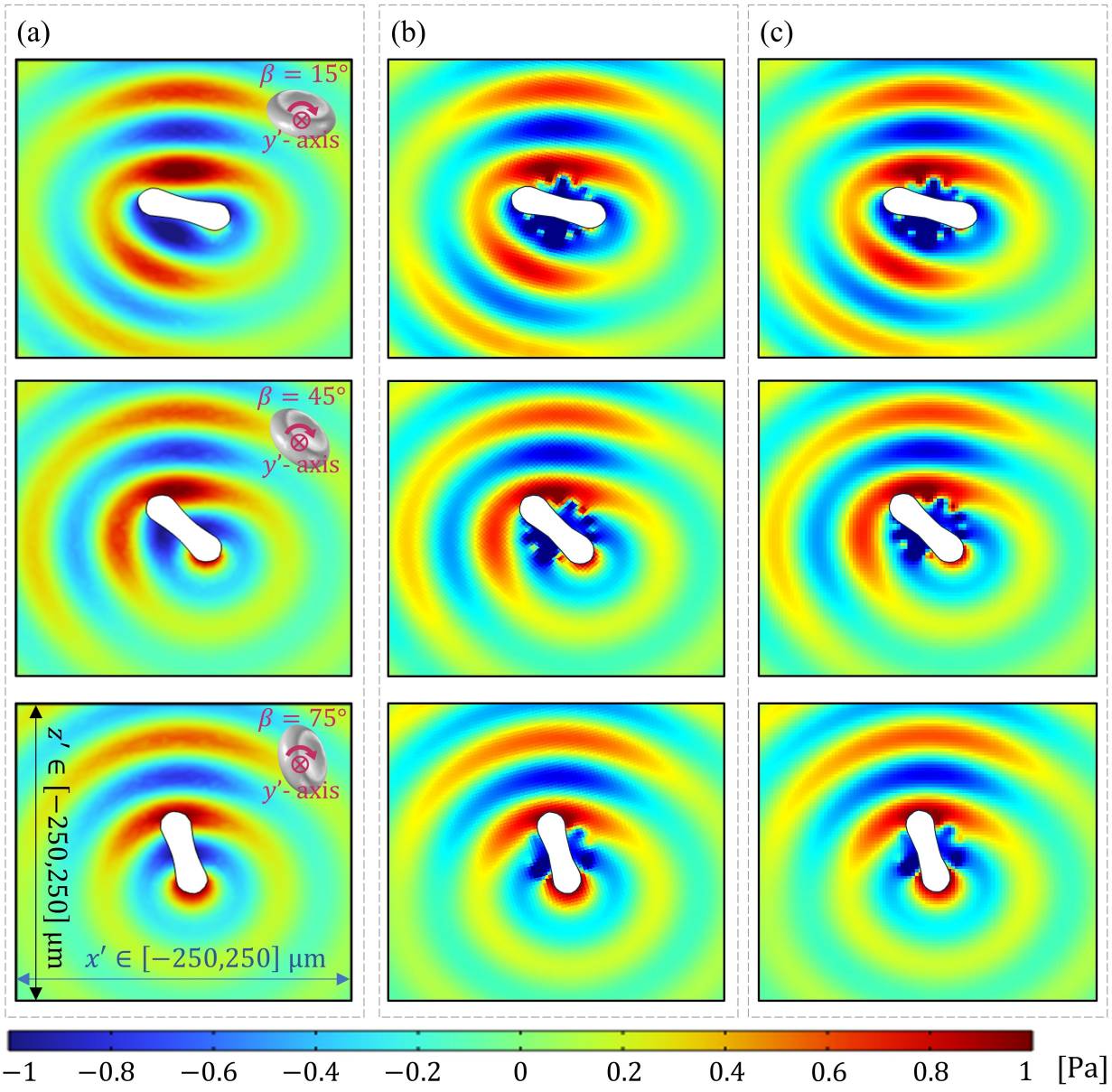

FIG. 5. The same as in Fig. 4, but with the scatterer replaced by a sound-soft disc-like object.

and rotation metrics are given in Eq. (17) and (22), respectively. The pressure amplitude can be solved from the potential amplitude using the relationship of $-\rho_0 \frac{\partial \phi}{\partial t} = p$. Theoretical calculations, employing the rotational transformation (RT, sub-figure (b)) and rotation matrices (RM, sub-figure (c)), are validated against three-dimensional numerical simulations (sub-figure (a)). A substantial agreement is observed in the scattering pressure amplitudes between our methods and the numerical simulations. In Eqs. (9) and (10), a conformal transformation is performed to map a non-spherical object to a sphere. Objects with greater deviation from the spherical shape require more complex combinations of mapping coefficients, c_n, which can lead to numerically unstable

calculations and distortions in the near-field acoustic fields. In contrast, as the mapping coordinate system asymptotically approaches the spherical coordinate system in the far-field, the prediction results show good agreement in regions where the distance from the object increases.

In the near-field region, noticeable discrepancies in the acoustic pressure amplitudes in Fig. 5 may arise due to mapping errors in the projection of non-spherical geometries onto a sphere through the conformal transformation approach. Given the substantial differences in geometric features between the disc-like object and a sphere, this introduces mapping errors during the near-field data transfer between the original and mapping coordinate systems. Conversely, the geometric similarities between the cone-like object and a sphere result in relatively small mapping errors. Consequently, errors in the near-field scattering field exist for the disc-like object, while ensuring a relatively accurate near-field scattering field for the cone-like object. It is crucial to note that the mapping coordinate system is specifically designed to asymptotically match the spherical coordinate system at the far-field[31]. As a result, accurate far-field information has been captured. Noted that the acoustic radiation force and torque depend on far-field information [referred to Eq. (11)], any inaccuracies in the near-field could not compromise the precision of these two parameters.

C. Comparison of radiation force and torque

In this section, we validate the theoretical evaluations of the acoustic radiation force and torque using Eqs. (18), (19), (24), and (25) with those calculations from full numerical simulations [referred to Eqs. (D.2) and (D.3) of work[31]] on the cone-like and the disc-like objects. Given the exceptionally small computed values for radiation force and torque, we have dimensionlessed these parameters to enhance visualization. Specifically, the radiation force efficiency is scaled as $\tilde{F}_{\mathrm{rad},i} = F_{\mathrm{rad},i}/[(\pi a^2 p_0^2)/(2\rho_0 c_0^2)],\ i = x',\ y',$ or z', and the radiation torque efficiency is scaled as $\tilde{T}_{\mathrm{rad},i} = T_{\mathrm{rad},i}/[(\pi a^3 p_0^2)/(2\rho_0 c_0^2)],\ i = x',\ y',$ or z'. Considering the axisymmetric nature, the acoustic radiation force on y'-axis, $F_{\mathrm{rad},y'}$, and the acoustic radiation torque on x'- and z'-axes, $T_{\mathrm{rad},x'}$ and $T_{\mathrm{rad},z'}$, are considerably weaker than their counterparts along other sensitive directions, i.e., $|F_{\mathrm{rad},x'}|$ or $|F_{\mathrm{rad},z'}| \gg F_{\mathrm{rad},y'} \approx 0$ and $|T_{\mathrm{rad},y'}| \gg T_{\mathrm{rad},x'}$ or $T_{\mathrm{rad},z'} \approx 0$. Therefore, our focus is directed towards plotting and discussing the acoustic radiation force efficiencies along the x'- and z'-axes, $\tilde{F}_{\mathrm{rad},x'}$ and $\tilde{F}_{\mathrm{rad},z'}$, as well as the acoustic radiation torque efficiency along the y'-axis, $\tilde{T}_{\mathrm{rad},y'}$. Observing Figs. 6 and 7, it is evident that the radiation force efficiency and torque efficiency obtained through our method [utilizing rotational transformation (RT) and rotation matrices (RM)]

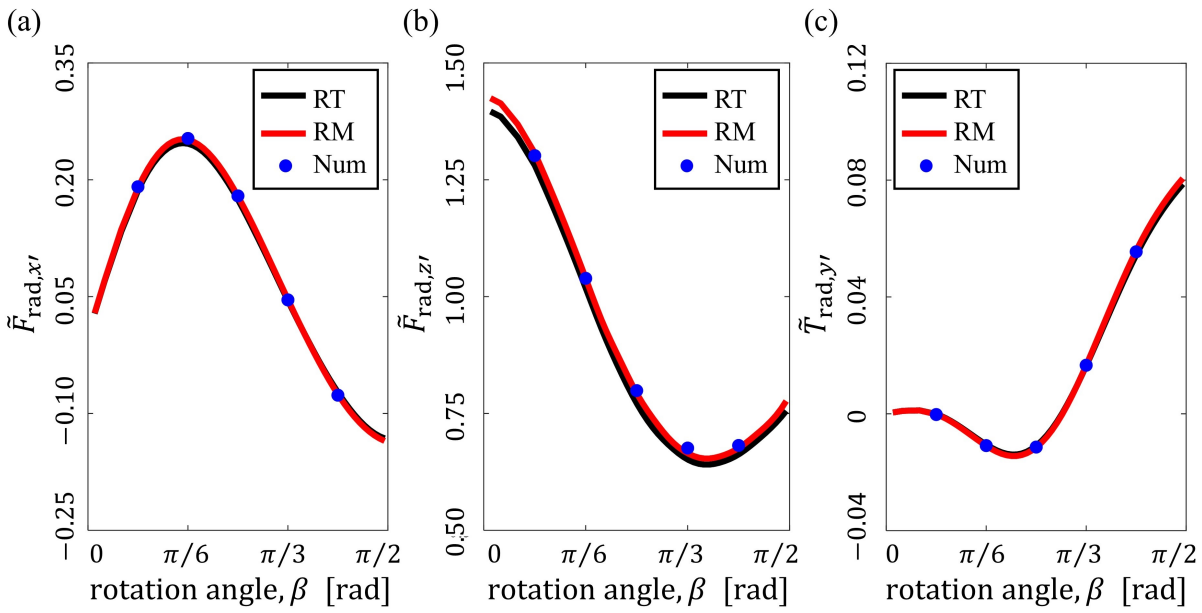

FIG. 6. Theoretical calculations [based on rotational transformation (RT) and rotation matrices (RM)] and numerical simulations (Num) of (a) the radiation force efficiency on the x'-axis [denoted as $\tilde{F}_{\mathrm{rad},x'}$], (b) the radiation force efficiency on the z'-axis [denoted as $\tilde{F}_{\mathrm{rad},z'}$], and (c) the radiation torque efficiency on the y'-axis [denoted as $\tilde{T}_{\mathrm{rad},y'}$], resulting from a unit plane wave ($p_0 = 1$ Pa) propagating along $+z'$-axis interacting with a sound-hard cone-like object with an average radius of $a = 50$ μm as a function of the rotationa angle, β.

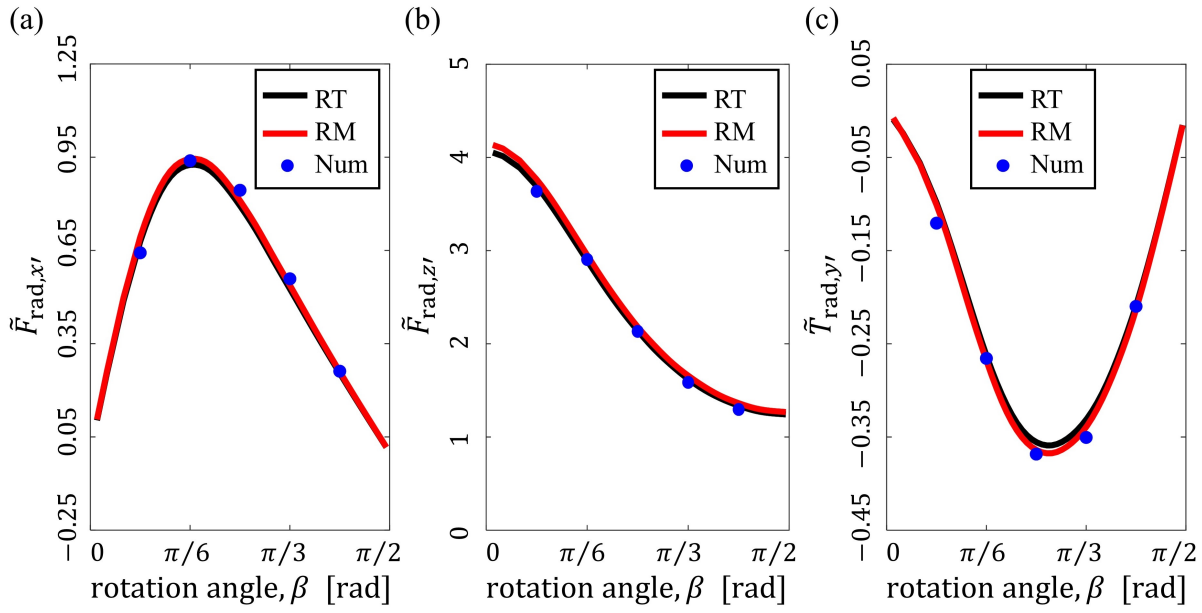

FIG. 7. The same as in Fig. 6, but with the scatterer replaced by a sound-soft disc-like object.

align well with the results from numerical simulations (Num) across varying rotational angles, β. It is noteworthy to reiterate that our formulations exhibit significantly shorter computational times compared to those reliant on the full finite-element method [approximately 1 second versus 10 minutes].

VI. CONCLUSIONS

In this study, we outline a theoretical framework based on partial-wave expansion series for the evaluation of acoustic scattering fields arising from the interaction between an incident wave and an axisymmetric object with arbitrary orientations. The derived scattering fields subsequently facilitate the computation of the radiation force and torque acting on the object.

Specifically, the conformal transformation approach is employed to integrate the influence of non-spherical geometric features into the calculations, while its applicability is limited to scenarios where the object is positioned at its standard orientation. Both rotational transformations and rotation addition theorem are crucial for addressing objects positioned at non-standard orientations The approach utilizing rotational transformation directly manipulates the solved acoustic fields, as well as the radiation force and torque, disrupting their inheritability within the partial-wave framework. In contrast, the method based on rotation addition theorem modulates the partial-wave expansion coefficients [including the beam-shape coefficients and the scalar scattering coefficients]. This ensures that the formulations of scattering products remain consistent and compact, which holds greater theoretical value. For instance, within the partial-wave framework, there is the potential to solve the multiple scattering fields, as well as the interaction radiation force and torque, in a system with multiple non-spherical objects, following a similar procedure as in a multi-sphere system[16,41]. Regarding computational accuracy, it can be observed that the scattering field [referred to Figs. 4 and 5] and the derived radiation force and torque [referred to Figs. 6 and 7] for different axisymmetric objects at various orientations can be effectively addressed with the assistance of either rotational transformation or rotation matrices. These results demonstrate a high level of agreement with full three-dimensional numerical simulations, yet the computational time is significantly lower than that of numerical method.

Considering the high computational accuracy and efficiency, the current study provides crucial theoretical support for manipulating axisymmetric objects at arbitrary orientations. In particular, due to the inherent consistency of the rotation addition theorem in computational format, there

is hope that the theoretical model originally designed for spherical objects could be seamlessly extended to axisymmetric objects.

Appendix A: Determination of radiation force and torque

The acoustic radiation force on an object due to scattering phenomena was obtained as a surface integration R, which should involve the object[4,5]:

$$\vec{F}_{\mathrm{rad}} = \int_{\mathrm{R}} \langle L \rangle \, \mathrm{d}\vec{\mathrm{A}}_{\mathrm{R}} - \rho_0 \int_{\mathrm{R}} \mathrm{d}\vec{\mathrm{A}}_{\mathrm{R}} \cdot \langle \vec{u}\vec{u} \rangle, \tag{A1}$$

where the angle bracket $\langle \cdot \rangle$ denotes the time average of the variable therein. L is the acoustic Lagrange density defined as $L = \frac{1}{2}\rho_0 \vec{u}\cdot\vec{u} - \frac{1}{2\rho_0 c^2} p^2$, where $\rho_0 \vec{u}\cdot\vec{u}$ is the flux of momentum density. The acoustic velocity and the acoustic pressure are decomposed as $\vec{u} = \vec{u}_{\mathrm{ex}} + \vec{u}_{\mathrm{sc}}$ and $p = p_{\mathrm{ex}} + p_{\mathrm{sc}}$, respectively. The spherical surface R surrounding the scattering particle is sufficiently far to involve the scatterer, and the direction of the integration element $\mathrm{d}\vec{\mathrm{A}}_{\mathrm{R}} = \mathrm{dA}_{\mathrm{R}}\vec{e}_r$ is along the outer normal of the surface. Three factors are now considered: (i) for the external incident wave which does not contribute to the radiation force, i.e., $\int_{\mathrm{R}} \langle L_{\mathrm{ex}} \rangle \, \mathrm{d}\vec{\mathrm{A}}_{\mathrm{R}} - \rho_0 \int_{\mathrm{R}} \mathrm{d}\vec{\mathrm{A}}_{\mathrm{R}} \cdot \langle \vec{u}_{\mathrm{ex}}\vec{u}_{\mathrm{ex}} \rangle = 0$; and (ii) the Sommerfeld radiation condition requires the acoustic Lagrange density for the scattering wave to satisfy $L_{\mathrm{sc}} = \frac{1}{2}\rho_0 \vec{u}_{\mathrm{sc}}\cdot\vec{u}_{\mathrm{sc}} - \frac{1}{2\rho_0 c^2} p_{\mathrm{sc}}^2 = 0$. Equation (A1) is reduced to

$$\vec{F}_{\mathrm{rad}} = \int_{\mathrm{R}} \frac{\rho_0 \omega^2}{c^2} \left[\langle \phi_{\mathrm{ex}} \phi_{\mathrm{sc}} \rangle \, \vec{e}_r + \langle \phi_{\mathrm{sc}} \phi_{\mathrm{sc}} \rangle + \left\langle \frac{\mathrm{i}c}{\omega} \phi_{\mathrm{sc}} \nabla \phi_{\mathrm{ex}} \right\rangle \right] \mathrm{dA}_{\mathrm{R}}, \tag{A2}$$

where $\vec{e}_r$ is the unit outer normal vector of the spherical surface R.

Using the relationship $\langle XY \rangle = \frac{1}{2}\mathrm{Re}\left(\hat{X}\hat{Y}^*\right)$, the force components in the Cartesian coordinate system can be expressed as $\vec{F}_{\mathrm{rad},x} = \vec{F}_{\mathrm{rad}} \cdot \vec{e}_x$, $\vec{F}_{\mathrm{rad},y} = \vec{F}_{\mathrm{rad}} \cdot \vec{e}_y$, $\vec{F}_{\mathrm{rad},z} = \vec{F}_{\mathrm{rad}} \cdot \vec{e}_z$ or

$$\begin{cases} \vec{F}_{\mathrm{rad},x} = \frac{\rho_0 \omega^2 R_0^2}{2c^2} \mathrm{Re} \int_0^{2\pi} \int_0^{\pi} \left[\left(\hat{\phi}_{\mathrm{ex}} - \frac{i}{k} \frac{\partial \hat{\phi}_{\mathrm{ex}}}{\partial r} \right) \hat{\phi}_{sc}^* + \left| \hat{\phi}_{\mathrm{sc}} \right|^2 \right] \cos(\varphi) \sin^2(\theta) \, d\theta d\varphi, \\ \vec{F}_{\mathrm{rad},y} = \frac{\rho_0 \omega^2 R_0^2}{2c^2} \mathrm{Re} \int_0^{2\pi} \int_0^{\pi} \left[\left(\hat{\phi}_{\mathrm{ex}} - \frac{i}{k} \frac{\partial \hat{\phi}_{\mathrm{ex}}}{\partial r} \right) \hat{\phi}_{sc}^* + \left| \hat{\phi}_{\mathrm{sc}} \right|^2 \right] \sin(\varphi) \sin^2(\theta) \, d\theta d\varphi, \\ \vec{F}_{\mathrm{rad},z} = \frac{\rho_0 \omega^2 R_0^2}{2c^2} \mathrm{Re} \int_0^{2\pi} \int_0^{\pi} \left[\left(\hat{\phi}_{\mathrm{ex}} - \frac{i}{k} \frac{\partial \hat{\phi}_{\mathrm{ex}}}{\partial r} \right) \hat{\phi}_{sc}^* + \left| \hat{\phi}_{\mathrm{sc}} \right|^2 \right] \cos(\theta) \sin(\theta) \, d\theta d\varphi. \end{cases} \tag{A3}$$

Considering that the integration spherical surface is far away from the object [i.e., $R_0 \to \infty$], the external and scattering potential amplitudes given in Eqs. (3) and (5) can be further simplified

using the relationships[11] $j_n(kr) \approx \frac{\sin\left(kr-\frac{\pi n}{2}\right)}{kr}$, $\frac{\partial[j_n(kr)]}{\partial r} \approx \frac{\cos\left(kr-\frac{\pi n}{2}\right)}{r}$, and $h_n^{(1)}(kr) \approx \frac{\mathrm{i}^{-(n+1)}\mathrm{e}^{\mathrm{i}kr}}{kr}$ as:

$$\begin{cases} \hat{\phi}_{\mathrm{ex}} = \sum_{n,m} a_{nm} Y_n^m(\theta,\phi) \frac{\sin\left(kr-\frac{\pi n}{2}\right)}{kr}, \\ \hat{\phi}_{\mathrm{sc}} = \sum_{n,m} a_{nm} s_{nm} Y_n^m(\theta,\phi) \frac{\mathrm{i}^{-(n+1)}\mathrm{e}^{\mathrm{i}kr}}{kr}, \\ \frac{\partial \hat{\phi}_{\mathrm{ex}}}{\partial r} = \sum_{n,m} a_{nm} Y_n^m(\theta,\phi) \frac{\cos\left(kr-\frac{\pi n}{2}\right)}{r}, \\ \hat{\phi}_{\mathrm{sc}}^* = \sum_{n,m} a_{nm}^* s_{nm}^* [Y_n^m(\theta,\phi)]^* \frac{\mathrm{i}^{(n+1)}\mathrm{e}^{-\mathrm{i}kr}}{kr}. \end{cases} \tag{A4}$$

Consequently, the acoustic radiation force on the irregular body can be evaluated by substituting Eq. (A4) into $\left(\hat{\phi}_{\mathrm{ex}} - \frac{i}{k}\frac{\partial \hat{\phi}_{\mathrm{ex}}}{\partial r}\right)\hat{\phi}_{\mathrm{sc}}^* + \left|\hat{\phi}_{\mathrm{sc}}\right|^2$, which yields:

$$\left(\hat{\phi}_{\mathrm{ex}} - \frac{i}{k}\frac{\partial \hat{\phi}_{\mathrm{ex}}}{\partial r}\right)\hat{\phi}_{\mathrm{sc}}^* + \left|\hat{\phi}_{\mathrm{sc}}\right|^2 = \frac{1}{(kr)^2}\sum_{n,m}\sum_{n\prime,m\prime} a_{nm}a_{n\prime m\prime}^*(1+s_{nm})s_{n\prime m\prime}^* Y_n^m(\theta,\phi)\left[Y_{n\prime}^{m\prime}(\theta,\phi)\right]^*. \tag{A5}$$

Additionally, considering the orthogonality and the recurrence properties of the spherical harmonics function[39], we have:

$$\begin{cases} \int_0^{2\pi}\int_0^{\pi} Y_n^m(\theta,\phi)\left[Y_{n\prime}^{m\prime}(\theta,\phi)\right]^* \cos(\varphi)\sin^2(\theta)\,\mathrm{d}\theta\mathrm{d}\varphi = \\ \qquad \frac{1}{2}\left(\mathscr{A}_{n+1}^{m+1}\delta_{n\prime,m+1}\delta_{m\prime,m+1} + \mathscr{B}_{n-1}^{m+1}\delta_{n\prime,n-1}\delta_{m\prime,m+1} + \mathscr{C}_{n+1}^{-m-1}\delta_{n\prime,n+1}\delta_{m\prime,m-1} + \mathscr{D}_{n-1}^{m-1}\delta_{n\prime,n-1}\delta_{m\prime,m-1}\right), \\ \int_0^{2\pi}\int_0^{\pi} Y_n^m(\theta,\phi)\left[Y_{n\prime}^{m\prime}(\theta,\phi)\right]^* \sin(\varphi)\sin^2(\theta)\,d\theta d\varphi = \\ \qquad \frac{-\mathrm{i}}{2}\left(\mathscr{A}_{n+1}^{m+1}\delta_{n\prime,m+1}\delta_{m\prime,m+1} + \mathscr{B}_{n-1}^{m+1}\delta_{n\prime,n-1}\delta_{m\prime,m+1} - \mathscr{C}_{n+1}^{-m-1}\delta_{n\prime,n+1}\delta_{m\prime,m-1} - \mathscr{D}_{n-1}^{m-1}\delta_{n\prime,n-1}\delta_{m\prime,m-1}\right), \\ \int_0^{2\pi}\int_0^{\pi} Y_n^m(\theta,\phi)\left[Y_{n\prime}^{m\prime}(\theta,\phi)\right]^* \cos(\theta)\sin(\theta)\,d\theta d\varphi = \frac{-\mathrm{i}}{2}\left(\mathscr{E}_{n+1}^{m}\delta_{n\prime,n+1}\delta_{m\prime,m-1} + \mathscr{F}_{n-1}^{m}\delta_{n\prime,n-1}\delta_{m\prime,m}\right), \end{cases} \tag{A6}$$

where δ_{nm} represents the Kronecker Delta. Finally, through inserting Eqs. (A5) and (A6) into Eq. (A3), we can explicitly express the acoustic radiation force as Eq. (12).

The acoustic radiation torque on an object has also been derived as a surface integration over the object[6]:

$$\vec{T}_{\mathrm{rad}} = -\rho_0 \int_{\mathrm{R}} \left\langle \left(\mathrm{d}\vec{\mathrm{A}}_{\mathrm{R}} \cdot \vec{u}\right) \cdot (\vec{r}\times\vec{u}) \right\rangle, \tag{A7}$$

Following relationships $-\rho_0\frac{\partial\phi}{\partial t} = p$ and $\nabla\phi = \vec{u}$, the potential form of Eq. (A7) is

$$\vec{T}_{\mathrm{rad}} = -\rho_0 \int_{\mathrm{R}} \left\langle \frac{\partial\phi}{\partial r} \cdot \mathrm{i}\vec{K}\phi \right\rangle \mathrm{dA}_{\mathrm{R}}, \tag{A8}$$

where $\vec{K} = -\mathrm{i}(\vec{r}\times\nabla)$ represents the angular momentum operator[39]. Similarly, we decompose the total potential field ϕ into the potential fields of external wave ϕ_{ex} and scattered wave ϕ_{sc} and

eliminate the time-averaged effects using relationship $\langle XY\rangle = \frac{1}{2}\mathrm{Re}\left(\hat{X}\hat{Y}^*\right)$. The acoustic torque given in Eq. (A8) becomes

$$\vec{T}_{\mathrm{rad}} = -\frac{\rho_0}{2}\mathrm{Re}\int_{\mathrm{R}}\left[\frac{\partial\hat{\phi}^*_{\mathrm{ex}}}{\partial r}\mathrm{i}\vec{K}\hat{\phi}_{\mathrm{sc}} - \hat{\phi}^*_{\mathrm{ex}}\mathrm{i}\vec{K}\frac{\partial\hat{\phi}_{\mathrm{sc}}}{\partial r} + \frac{\partial\hat{\phi}^*_{\mathrm{sc}}}{\partial r}\mathrm{i}\vec{K}\hat{\phi}_{\mathrm{sc}}\right]\mathrm{dA_R}. \tag{A9}$$

Considering the partial-wave expressions of Eqs. (3) and (5), we have:

$$\begin{cases}
\frac{\partial\hat{\phi}^*_{\mathrm{ex}}}{\partial r}\vec{K}\hat{\phi}_{\mathrm{sc}} = k\sum_{n,m}\sum_{n',m'}\ a_{nm}a^*_{n'm'}s_{nm}h^{(1)}_n(kr)\frac{\partial[j_{n\prime}(kr)]}{\partial r}\left\{\left[Y^{m\prime}_{n\prime}(\theta,\phi)\right]^*\left[\vec{K}Y^m_n(\theta,\phi)\right]\right\},\\
\hat{\phi}^*_{\mathrm{ex}}\vec{K}\frac{\partial\hat{\phi}_{\mathrm{sc}}}{\partial r} = k\sum_{n,m}\sum_{n',m'}a_{nm}a^*_{n'm'}s_{nm}j_{n\prime}(kr)\frac{\partial\left[h^{(1)}_n(kr)\right]}{\partial r}\left\{\left[Y^{m\prime}_{n\prime}(\theta,\phi)\right]^*\left[\vec{K}Y^m_n(\theta,\phi)\right]\right\},\\
\frac{\partial\hat{\phi}^*_{\mathrm{sc}}}{\partial r}\vec{K}\hat{\phi}_{\mathrm{sc}} = k\sum_{n,m}\sum_{n',m'}a_{nm}a^*_{n'm'}s_{nm}s^*_{n'm'}h^{(1)}_n(kr)\frac{\partial\left[h^{(1)}_{n\prime}(kr)\right]^*}{\partial r}\left\{\left[Y^{m\prime}_{n\prime}(\theta,\phi)\right]^*\left[\vec{K}Y^m_n(\theta,\phi)\right]\right\}.
\end{cases} \tag{A10}$$

Substituting Eq. (A10) into Eq. (A9), we yield:

$$\begin{aligned}
\vec{T}_{\mathrm{rad}} =& \frac{k\rho_0}{2}\mathrm{Im}\int_{\mathrm{R}}\sum_{n,m}\sum_{n',m'}\left\{\left[Y^{m\prime}_{n\prime}(\theta,\phi)\right]^*\left[\vec{K}Y^m_n(\theta,\phi)\right]\right\}(a_{nm}a^*_{n'm'}s_{nm})\\
&\left\{h^{(1)}_n(kr)\frac{\partial\left[j_{n\prime}(kr)\right]}{\partial r} - j_{n\prime}(kr)\frac{\partial\left[h^{(1)}_n(kr)\right]}{\partial r} + s^*_{n'm'}h^{(1)}_n(kr)\frac{\partial\left[h^{(1)}_{n\prime}(kr)\right]^*}{\partial r}\right\}\mathrm{dA_R}.
\end{aligned} \tag{A11}$$

For the far-field region, we further simplify the above equation using the relationships[11] $j_n(kr)\approx\frac{\sin\left(kr-\frac{\pi n}{2}\right)}{kr}$, $\frac{\partial[j_n(kr)]}{\partial r}\approx\frac{\cos\left(kr-\frac{\pi n}{2}\right)}{r}$, $h^{(1)}_n(kr)\approx\frac{\mathrm{i}^{-(n+1)}\mathrm{e}^{\mathrm{i}kr}}{kr}$, $\left[h^{(1)}_n(kr)\right]^*\approx\frac{\mathrm{i}^{(n+1)}\mathrm{e}^{-\mathrm{i}kr}}{kr}$, $\frac{\partial\left[h^{(1)}_n(kr)\right]}{\partial r}\approx\frac{\mathrm{i}^{-n}\mathrm{e}^{\mathrm{i}kr}}{kr}$, and $\frac{\partial\left[h^{(1)}_n(kr)\right]^*}{\partial r}\approx\frac{\mathrm{i}^{n}\mathrm{e}^{-\mathrm{i}kr}}{kr}$, as:

$$\vec{T}_{\mathrm{rad}} = -\frac{\rho_0}{2kR_0^2}\mathrm{Re}\int_{\mathrm{R}}\sum_{n,m}\sum_{n',m'}\left\{\left[Y^{m\prime}_{n\prime}(\theta,\phi)\right]^*\left[\vec{K}Y^m_n(\theta,\phi)\right]\right\}(a_{nm}a^*_{n'm'}s_{nm})\,\mathrm{i}^{(n'-n)}(1+s^*_{n'm'})\mathrm{dA_R}. \tag{A12}$$

Finally, with the help of relationships[39] $(K_x\pm\mathrm{i}K_y)Y^m_n(\theta,\varphi) = \mathscr{G}^m_nY^{m\pm1}_n(\theta,\varphi)$ and $K_zY^m_n(\theta,\varphi) = mY^m_n(\theta,\varphi)$ [K_x, K_y, and K_z are the Cartesian components of $\vec{K}$], we have:

$$\begin{cases}
T_{\mathrm{rad},x}\pm\mathrm{i}T_{\mathrm{rad},y} = \frac{\rho_0}{2k}\mathrm{Re}\sum_{n,m}\mathscr{G}^{\pm m}_n a_{n,m\mp1}a^*_{nm}s_{n,m\mp1}(1+s^*_{nm}),\\
T_{\mathrm{rad},z} = \frac{\rho_0}{2k}\mathrm{Re}\sum_{n,m}ma_{nm}a^*_{nm}s_{nm}(1+s^*_{nm}).
\end{cases} \tag{A13}$$

Based on Eq. (A13), e acoustic radiation torque on the irregular body can be explicitly formulated in the Cartesian coordinate system as shown in Eq. (13).

Appendix B: Determination of rotation matrices

Suppose that a set of Cartesian axes $Ox'y'z'$ is rotated into axes $Oxyz$ following the finite rotational principles, and the rotation angle is $\vec{\theta}_{\rm rot} = (\alpha, \beta, \gamma)$. It should be further emphasized that by employing the rotational concept, the components of radiation force (or torque) can be expressed in a unified format. This is achieved by rotating the coordinate system and utilizing rotation matrices to transform the coefficients[42]. Based on the addition theorem[37,42], the effects of rotations is enforced on the spherical harmonics function as

$$Y_n^m(\theta,\phi) = \sum_{l=-n}^{+n} D_n^{m,l}(\vec{\theta}_{\rm rot}) Y_n^m(\theta',\phi'), \tag{B1}$$

and the entries of rotation matrices $D_n^{m,l}(\vec{\theta}_{\rm rot})$ can be calculated by

$$D_n^{m,l}(\alpha,\beta,\gamma) = \mathrm{e}^{-\mathrm{i}l\alpha} d_n^{m,l}(\beta) \mathrm{e}^{-\mathrm{i}l\gamma}, \tag{B2}$$

where the reduced rotation matrices $d_n^{m,l}(\beta)$ satisfy[43]

$$d_n^{m,l}(\beta) = (-1)^{m+l} U_n^{m,l} \left(\frac{\beta}{2}\right) \sqrt{\frac{(n+l)!(n-l)!}{(n+m)!(n-m)!}}, \tag{B3}$$

with entities $U_n^{m,l}(\tau)$ are defined as

$$\begin{aligned} &U_n^{m,l}(\tau) = (-1)^{n+l} C_{n+m}^{n-l} (\cos\tau)^{l+m} (\sin\tau)^{l-m} F_{l-n,n+l+1}^{l+m+1}\left(\cos^2\tau\right) \\ &(\text{for } \; l+m \geq 0) \end{aligned}, \tag{B4}$$

where $C_n^m = \frac{n!}{m!(n-m)!}$ and $F_{n,m}^l(x)$ are the binomial coefficients and the hypergeometric function, respectively.

In order to explicitly express the hypergeometric function, we introduce the Jacobi polynomial, given by

$$P_N^{(a,b)}(\cos 2\tau) = \frac{1}{2^N} \sum_{k=0}^{N} C_{N+a}^{N-k} C_{N+b}^{k} (\cos 2\tau - 1)^k (\cos 2\tau + 1)^{N-k}. \tag{B5}$$

Considering that the Jacobi polynomial can be represented by the hypergeometric function by[44]

$$P_N^{(a,b)}(\cos 2\tau) = \frac{(-1)^N (N+b)!}{N! b!} F_{-N,N+a+b+1}^{b+1}\left(\cos^2\tau\right), \tag{B6}$$

the hypergeometric function in Eq. (B4) for $l+m \geq 0$ can be solved by equating Eqs. (B5) and (B6) [replacing $N = n-l$, $a = l-m$, and $b = l+m$]:

$$\begin{aligned} F_{l-n,n+l+1}^{l+m+1}\left(\cos^2\tau\right) &= \left[\sum_{k=0}^{n-l} \frac{(n-m)!(n+m)!}{(n-l-k)!(l+k-m)!(n+m-k)!k!}(-1)^k(\cos\tau)^{2n-2l}(\tan\tau)^{2k}\right] \frac{(n-l)!(l+m)!}{(-1)^{n-l}(n+m)!} \\ &= \sum_{k=0}^{n-l}(-1)^{k+l-n}\frac{(n-m)!(n-l)!(l+m)!}{(n-l-k)!(l+k-m)!(n+m-k)!k!}(\cos\tau)^{2n-2l}(\tan\tau)^{2k}, \end{aligned} \tag{B7}$$

Thus, inserting Eq. (B7) into Eq. (B4), we have

$$\begin{aligned} &U_n^{m,l}(\tau) = \sum_{k=0}^{n-l}(-1)^k\frac{(n-m)!(n+m)!}{(n-l-k)!(l+k-m)!(n+m-k)!k!}(\cos\tau)^{2n}(\tan\tau)^{2k+l-m} \\ &(\text{for } \; l+m \geq 0) \end{aligned} . \tag{B8}$$

Finally, we obtain the explicit expression of the reduced rotation matrices by insert Eq. (B8) into Eq. (B3), which is

$$\begin{aligned} &d_n^{m,l}(\beta) = \sum_{k=0}^{n-l}(-1)^{k+l+m}\frac{\sqrt{(n+l)!(n-l)!(n+m)!(n-m)!}}{(n-l-k)!(l+k-m)!(n+m-k)!k!}\left(\cos\frac{\beta}{2}\right)^{2n}\left(\tan\frac{\beta}{2}\right)^{2k+l-m} \\ &(\text{for } \; l+m \geq 0) \end{aligned} . \tag{B9}$$

Note that Eq. (B9) can be only used to evaluate the reduced rotation matrices when $l+m \geq 0$; for other values of l and m, we can use

$$\begin{aligned} &d_n^{m,l}(\beta) = (-1)^{m+l}d_n^{-m,-l}(\beta) \\ &(\text{for } \; l+m < 0) \end{aligned} , \tag{B10}$$

with $d_n^{-m,-l}(\beta)$ is evaluated by Eq. (B9) since $(-l)+(-m) \geq 0$. Once the reduced rotation matrices $d_n^{m,l}(\beta)$ is determined, the rotation matrices $D_n^{m,l}(\vec{\theta}_{\text{rot}})$ [or $D_n^{m,l}(\alpha,\beta,\gamma)$] can be calculated by Eq. (B2).

CONFLICT OF INTEREST STATEMENT

The authors declared that they have no conflicts of interest to this work.

DATA AVAILABILITY

The authors confirm that the data supporting the findings of the conclusions are available within the article.

ACKNOWLEDGMENTS

This work is supported by the following funding organizations in China: GuangDong Basic and Applied Basic Research Foundation (Grant Number 2023A1515110927), National Natural Science Foundation of China (Grant Number 52105090).

REFERENCES

[1]D. Ahmed, A. Ozcelik, N. Bojanala, N. Nama, A. Upadhyay, Y. Chen, W. Hanna-Rose, and T. J. Huang, "Rotational manipulation of single cells and organisms using acoustic waves," Nature communications **7**, 11085 (2016).

[2]A. Marzo, S. A. Seah, B. W. Drinkwater, D. R. Sahoo, B. Long, and S. Subramanian, "Holographic acoustic elements for manipulation of levitated objects," Nature communications **6**, 8661 (2015).

[3]A. Marzo and B. W. Drinkwater, "Holographic acoustic tweezers," Proceedings of the National Academy of Sciences **116**, 84–89 (2019).

[4]P. J. Westervelt, "The theory of steady forces caused by sound waves," The Journal of the Acoustical Society of America **23**, 312–315 (1951).

[5]P. J. Westervelt, "Acoustic radiation pressure," The Journal of the Acoustical Society of America **29**, 26–29 (1957).

[6]G. Maidanik, "Torques due to acoustical radiation pressure," The Journal of the Acoustical Society of America **30**, 620–623 (1958).

[7]Z. Fan, D. Mei, K. Yang, and Z. Chen, "Acoustic radiation torque on an irregularly shaped scatterer in an arbitrary sound field," The Journal of the Acoustical Society of America **124**, 2727–2732 (2008).

[8]L. Zhang and P. L. Marston, "Acoustic radiation torque and the conservation of angular momentum (l)." The Journal of the Acoustical Society of America **129**, 1679–1680 (2011).

[9]L. P. Gor'kov, "On the forces acting on a small particle in an acoustical field in an ideal fluid," Soviet Physics Doklady **6**, 773–775 (1962).

[10]T. Tang, B. Dong, and L. Huang, "Agglomeration of particles by a converging ultrasound field and their quantitative assessments," Ultrasonics sonochemistry **75**, 105590 (2021).

[11]E. G. Williams, *Fourier acoustics: sound radiation and nearfield acoustical holography* (Academic press, 1999).

[12]G. T. Silva, "Acoustic radiation force and torque on an absorbing compressible particle in an inviscid fluid," The Journal of the Acoustical Society of America **136**, 2405–2413 (2014).

[13]L. Zhang and P. L. Marston, "Geometrical interpretation of negative radiation forces of acoustical bessel beams on spheres," Physical Review E **84**, 035601 (2011).

[14]Z. Gong and M. Baudoin, "Equivalence between angular spectrum-based and multipole expansion-based formulas of the acoustic radiation force and torque," The Journal of the Acoustical Society of America **149**, 3469–3482 (2021).

[15]J. Wang, F. Cai, Q. Lin, D. Zhao, and H. Zheng, "Acoustic radiation force dependence on properties of elastic spherical shells in standing waves," Ultrasonics **127**, 106836 (2023).

[16]T. Tang and L. Huang, "Acoustic radiation force for multiple particles over a wide size-scale by multiple ultrasound sources," Journal of Sound and Vibration **509**, 116256 (2021).

[17]P. L. Marston, "Shape oscillation and static deformation of drops and bubbles driven by modulated radiation stressestheory," The Journal of the Acoustical Society of America **67**, 15–26 (1980).

[18]P. L. Marston and R. E. Apfel, "Quadrupole resonance of drops driven by modulated acoustic radiation pressureexperimental properties," The Journal of the Acoustical Society of America **67**, 27–37 (1980).

[19]L. Huang, S.-C. Bao, F. Cai, L. Meng, W. Zhou, J. Zhou, D. Kong, F. Li, and H. Zheng, "Acoustic rotation of multiple subwavelength cylinders for three-dimensional topography reconstruction," Journal of Applied Physics **134** (2023).

[20]T. Tang, C. Shen, and L. Huang, "Acoustic rotation of non-spherical micro-objects: Characterization of acoustophoresis and quantification of rotational stability," Journal of Sound and Vibration **554**, 117694 (2023).

[21]B. T. Hefner and P. L. Marston, "An acoustical helicoidal wave transducer with applications for the alignment of ultrasonic and underwater systems," The Journal of the Acoustical Society of America **106**, 3313–3316 (1999).

[22]L. Zhang and P. L. Marston, "Angular momentum flux of nonparaxial acoustic vortex beams and torques on axisymmetric objects," Physical Review E **84**, 065601 (2011).

[23]L. Zhang and P. L. Marston, "Acoustic radiation torque on small objects in viscous fluids and connection with viscous dissipation," The Journal of the Acoustical Society of America **136**, 2917–2921 (2014).

[24]L. Zhang, "Reversals of orbital angular momentum transfer and radiation torque," Physical Review Applied **10**, 034039 (2018).

[25]F. Mitri, "Radiation forces and torque on a rigid elliptical cylinder in acoustical plane progressive and (quasi) standing waves with arbitrary incidence," Physics of Fluids **28** (2016).

[26]F. Mitri, "Axial acoustic radiation force on rigid oblate and prolate spheroids in bessel vortex beams of progressive, standing and quasi-standing waves," Ultrasonics **74**, 62–71 (2017).

[27]P. L. Marston, "Comment on radiation forces and torque on a rigid elliptical cylinder in acoustical plane progressive and (quasi) standing waves with arbitrary incidence[phys. fluids 28, 077104 (2016)]," Physics of Fluids **29** (2017).

[28]E. B. Lima, J. P. Leão-Neto, A. S. Marques, G. C. Silva, J. H. Lopes, and G. T. Silva, "Nonlinear interaction of acoustic waves with a spheroidal particle: Radiation force and torque effects," Physical Review Applied **13**, 064048 (2020).

[29]D. T. DiPerna and T. K. Stanton, "Sound scattering by cylinders of noncircular cross section: A conformal mapping approach," The Journal of the Acoustical Society of America **96**, 3064–3079 (1994).

[30]D. B. Reeder and T. K. Stanton, "Acoustic scattering by axisymmetric finite-length bodies: An extension of a two-dimensional conformal mapping method," The Journal of the Acoustical Society of America **116**, 729–746 (2004).

[31]T. Tang and L. Huang, "An efficient semi-analytical procedure to calculate acoustic radiation force and torque for axisymmetric irregular bodies," Journal of Sound and Vibration **532**, 117012 (2022).

[32]T. Tang, G. T. Silva, L. Huang, and X. Han, "Acoustic levitation of axisymmetric mie objects above a transducer array by engineering the acoustic radiation force and torque," Physical Review E **106**, 045108 (2022).

[33]T. Tang, C. Shen, and L. Huang, "Propagation of acoustic waves and determined radiation effects on axisymmetric objects in heterogeneous medium with irregular interfaces," Physics of Fluids **36** (2024).

[34]T. Tang and L. Huang, "Theoretical framework to predict the acoustophoresis of axisymmetric irregular objects above an ultrasound transducer array," Physical Review E **105**, 055110 (2022).

[35]T. Tang and L. Huang, "Soundiation: A software in evaluation of acoustophoresis driven by radiation force and torque on axisymmetric objects," The Journal of the Acoustical Society of America **152**, 2934–2945 (2022).

[36]T. Tang, *Acoustic manipulation of micro-objects*, Ph.D. thesis, The University of Hong Kong (2022).

[37]P. A. Martin, *Multiple scattering: interaction of time-harmonic waves with N obstacles*, 107 (Cambridge University Press, 2006).

[38]G. T. Silva, "Off-axis scattering of an ultrasound bessel beam by a sphere," IEEE transactions on ultrasonics, ferroelectrics, and frequency control **58**, 298–304 (2011).

[39]G. B. Arfken, H. J. Weber, and F. E. Harris, *Mathematical methods for physicists: a comprehensive guide* (Academic press, 2011).

[40]J. E. Gentle, *Matrix algebra* (Springer, New York, 2007).

[41]J. H. Lopes, M. Azarpeyvand, and G. T. Silva, "Acoustic interaction forces and torques acting on suspended spheres in an ideal fluid," IEEE transactions on ultrasonics, ferroelectrics, and frequency control **63**, 186–197 (2015).

[42]Y. A. Ilinskii, E. A. Zabolotskaya, B. C. Treweek, and M. F. Hamilton, "Acoustic radiation force on an elastic sphere in a soft elastic medium," The Journal of the Acoustical Society of America **144**, 568–576 (2018).

[43]R. Courant and D. Hilbert, *Methods of mathematical physics* (New York: Interscience, 1953).

[44]I. S. Gradshteyn and I. M. Ryzhik, *Table of Integrals, Series, and Products* (New York: Academic Press, 1980).